

석사학위논문
Master Thesis

입자법을 이용한 수중폭발 수치해석
시뮬레이션

Numerical simulation of underwater explosion using
Smoothed Particle Hydrodynamics

2017

박형준 (朴炯濬 Park, Hyung Jun)

한국과학기술원

Korea Advanced Institute of Science and Technology

석사학위논문

입자법을 이용한 수중폭발 수치해석
시뮬레이션

2017

박형준

한국과학기술원

기계항공공학부/기계공학과

입자법을 이용한 수중폭발 수치해석 시뮬레이션

박 형 준

위 논문은 한국과학기술원 석사학위논문으로
학위논문 심사위원회의 심사를 통과하였음

2016년 12월 26일

심사위원장 이 필 승 (인)

심사위원 김 대 겸 (인)

심사위원 황 성 철 (인)

Numerical simulation of underwater explosion using Smoothed Particle Hydrodynamics

Park, Hyung Jun

Advisor: Lee, Phill-Seung

A thesis submitted to the faculty of
Korea Advanced Institute of Science and Technology in
partial fulfillment of the requirements for the degree of
Master of Science in Mechanical Engineering

Daejeon, Korea
December 26, 2016

Approved by

Lee, Phill-Seung
Professor of Mechanical Engineering

The study was conducted in accordance with Code of Research Ethics¹⁾.

1) Declaration of Ethical Conduct in Research: I, as a graduate student of Korea Advanced Institute of Science and Technology, hereby declare that I have not committed any act that may damage the credibility of my research. This includes, but is not limited to, falsification, thesis written by someone else, distortion of research findings, and plagiarism. I confirm that my dissertation contains honest conclusions based on my own careful research under the guidance of my advisor.

MME
201532780

박형준. 입자법을 이용한 수중폭발 수치해석 시뮬레이션.
기계항공공학부/기계공학과. 2017년. 47+v 쪽. 지도교수:
이필승. (영문 논문)

Park, Hyung Jun. Numerical simulation of underwater explosion
using Smoothed Particle Hydrodynamics. School of Mechanical and
Aerospace Engineering/Department of Mechanical Engineering.
2017. 47+v pages. Advisor: Lee, Phill-Seung. (Text in English)

초 록

수중폭발은 충격파, 거스버블 맥동, 버블 제트와 같은 다양한 물리현상을 유발한다. 이와 같은 현상은 고압, 대 변형, 다 상, 다 경계로 구성된 복잡한 문제이다. 본 학위논문에서는 수중폭발의 전 과정을 시뮬레이션 하기 위하여 라그랑지안 기반의 입자법인 SPH(Smoothed Particle Hydrodynamics)를 적용 하였다. 충격파와 가스 버블의 물리현상은 각각 다른 시간단위를 가지며 또한 다른 상태방정식이 이용된다. 이와 같은 이유로, 각 현상에 대한 수치적 모듈이 분리되어 제시 되었으며, 모듈이 전환되는 전이점을 얻기 위한 방법이 제시 되었다. 또한, 가스버블 맥동현상의 구현을 위하여 수정된 상태방정식을 제안하였다. 수치해석 모델의 검증은 실험식, 타 수치기법, 그리고 실험과의 비교를 통해 수행되었다.

핵 심 낱 말 수중폭발, 충격파, 가스버블, 입자법, 수치해석

Abstract

Underwater explosion generates various physical phenomena such as shock wave, bubble pulsation and bubble jet. These phenomena involve complicated problems, which consist of high pressure, large deformation and multi-interface flow, etc. In this study, a Lagrangian meshless method, smoothed particle hydrodynamics(SPH) is applied to simulate the whole process of underwater explosion. It has different time scale and equation of state for pressure term between shock physics and bubble dynamics in standard SPH formulation. For this reason, numerical modules for each phenomenon are presented separately, and a method for obtaining the transition point where the module is converted is proposed. In addition, a modified state equation is presented to implement the gas bubble pulsation phenomenon. The numerical model verification is performed via comparing with empirical formulas, other numerical methods, and experiments.

Keywords underwater explosion, shock physics, bubble dynamics, SPH, numerical analysis

Contents

Contents	i
List of Tables	iii
List of Figures	iv
Chapter 1. Introduction	1
1.1 Research Background	1
1.2 Research Purpose	2
Chapter 2. Methodology	3
2.1 Underwater Explosion Phenomena	3
2.1.1 Shock Wave	3
2.1.2 Bubble Dynamics	4
2.2 Formulation of SPH Method	5
2.2.1 Integral Representation	5
2.2.2 Particle Approximation	6
2.2.3 Kernel Function	8
2.3 Numerical Approximation	9
2.3.1 Governing Equation	9
2.3.2 Viscosity	10
2.4 SPH Implementation	11
2.4.1 Tree-Search Algorithm	11
2.4.2 Boundary Conditions	13
2.4.3 Interface Sharpness Treatment	14
2.4.4 Time Integration Scheme	14
2.5 Equation of State for Pressure	15
2.5.1 Pressure Equation for Shock Physics	16

2.5.2 Pressure Equation for Bubble Dynamics	16
2.6 Transition Point.....	17
Chapter 3. Numerical Results	20
3.1 Dam Breaking Simulation	20
3.2 Shock Wave Simulation.....	24
3.3 Bubble Rising Simulation.....	30
3.4 Transition Point Verification.....	34
3.5 Bubble Pulsation Simulation	38
Chapter 4. Concluding Remark	43
Chapter 5. Bibliography	44
Chapter 6. Acknowledgments in Korean	46
Chapter 7. Curriculum Vitae in Korean	47

List of Tables

Table 2.1. Computational cost comparison of between searching algorithms.	12
Table 3.1. Parameters for bubble rising simulation.	30
Table 3.2. Parameters for each case.	35
Table 3.3. Maximum radius and initial period comparison between the Rayleigh-Plesset equation and the empirical formula.	37
Table 3.4. Numerical model parameters for 2D CASE and 3D CASE.	38

List of Figures

Figure 2.1. Shock wave propagtation.	3
Figure 2.2. Behavior of bubble pulsation and bubble jet.	4
Figure 2.3. Kernerl function model with support domain, Ω	7
Figure 2.4. Tree structure about whole domain.	12
Figure 2.5. Classification of each physical phenomenon.	17
Figure 2.6. Flow chart for describing a method for obtaining the transition point.	18
Figure 3.1. Numerical model of dam breaking simulation.	20
Figure 3.2. Comparison of a experiment and SPH. Left : progression of water over time. Right : Elevation of water column over time. Blue dot : experimental result. Green dot : SPH result of 1800 particles. Red dot : SPH result of 800 particles.	21
Figure 3.3. Dam breaking simulation from initial stage to 0.9 s.	22
Figure 3.4. Dam breaking simulation from 1.2 s to 2.1 s.	23
Figure 3.5. Numerical model of free field shock wave simulation.	24
Figure 3.6. Shock wave simulation from initial stage to 100 μs . Left : particle behavior. Right : pressure distribution.	25
Figure 3.7. Shock wave simulation from 200 μs to 300 μs . Left : particle behavior. Right : pressure distribution.	26
Figure 3.8. Shock wave simulation from 400 μs to 500 μs . Left : particle behavior. Right : pressure distribution.	27
Figure 3.9. Shock wave simulation from 600 μs to 700 μs . Left : particle behavior. Right : pressure distribution.	28
Figure 3.10. Comparison curve of shock wave pressure at gauging point 1 and point 2. Upper graph represents the gauging point 1 while lower graph shows the gauging point 2.	29
Figure 3.11. Numerical model of the bubble rising simulation. Green line represents wall boundary.	31
Figure 3.12. Comparison of bubble rising behavior from $t\sqrt{g/R} = 2.8$ to $t\sqrt{g/R} = 4.0$. Blue diamonds correspond to the Level-Set method[20] and black line represents SPH method proposed by Grenier[4]. Sky blue dots show the present SPH result.	32

Figure 3.13. Comparison of bubble rising behavior from $t \sqrt{g/R} = 4.4$ to $t \sqrt{g/R} = 5.6$. Blue diamonds correspond to the Level-Set method[20] and black line represents SPH method proposed by Grenier[4]. Sky blue dots show the present SPH result.....	33
Figure 3.14. 3D shock wave simulation in three viewpoints. Clockwise from the top, view(-37.5, 30.0), half of view(-37.5, 30.0), view(0.0, 90.0).	34
Figure 3.15. Log scale pressure comparison curve between empirical and numerical for CASE 1.	35
Figure 3.16. Rayleigh-Plesset curve for CASE 1.	36
Figure 3.17. Log scale pressure comparison curve between empirical and numerical for CASE 2.	36
Figure 3.18. Rayleigh-Plesset curve for CASE 2.	37
Figure 3.19. Numerical model of bubble pulsation	39
Figure 3.20. Numerical results of a 55g explosive charge.....	39
Figure 3.21. Numerical 2D(approximation) and 3D bubble volume profile for the explosive charge of 55g TNT.	40
Figure 3.22. Time history of bubble volume with different number of particles. And comparison with experiments and BEM[9].....	41
Figure 3.23. Time history of bubble volume with different amount of explosive charge. And comparison with experiments and BEM[9].....	42

Chapter 1. Introduction

1.1 Research Background

Underwater explosion is one of major issues in modern naval battles. Most related studies have been performed by analytical or experimental methods. Analytical solutions are limited only to simple cases due to the complex physics phenomena. Experimental researches are very expensive and dangerous. For this reason, Numerical simulation can be a good alternative to get solution.

For conventional grid-based numerical simulation methods such as FEM, FDM, It has a difficulty to deal with the underwater explosion problem. The underwater explosion generates shock wave, bubble pulsation and bubble jet. These phenomena are extremely complex problems, which involve high pressure and velocity, large deformation and distortion, multi-interface and multi-phase flow[10-13]. Recently more and more interests are focused on the meshless methods to deal with above-mentioned problems. In this paper, one of meshless methods, Smoothed Particle Hydrodynamics method(SPH) is considered to solve the problems due to several reasons.

SPH is a particle-based method of pure Lagrangian characteristic. Each particle is used as interpolation points to represent physics values. Since based on particles, there is no mesh and connectivity among each point. It can not only easily express multi-interface, free surface, but also overcome problem of large deformation. These characteristics make SPH suitable to simulate the underwater explosion.

SPH was invented to solve astrophysical problems by Lucy and his cooperator[3]. Since invention, SPH has been studied in various fields. In the field of explosion, Liu and his coworker[12,13] performed 1-dimensional explosive detonation simulation and 2-dimensional free field underwater explosion simulation using SPH. However, it is restricted only for simulating the shock wave problem. Although A. Zhang et al.[26] developed the combination model of SPH and boundary element method to express the whole process of underwater explosion including bubble dynamics, there is not enough reason to explain validity of connection between SPH and BEM(boundary element method). For multi-phase flow with small density ratio, Colagrossi and Landrini[1] proposed modified SPH formulation. In their works, the 2-dimensional bubble rising and dam breaking problem is only considered. Das and Das[2] simulated 3-dimensional bubble necking problem at the

submerged orifice. It was mainly focused on the bubbles separated from the orifice. A. Zhang et al. [24] simulated 3-D rising bubbles and coalescence of them. But they didn't focus on the bubble pulsation. The bubble pulsation problem is different from the bubble rising problem since the compressibility of the gas bubble during the pulsation process.

Until now, the multi-phase flow simulation that one more phase is considered the large compressibility has not been presented in the field of SPH. To express the bubble pulsation which is one of the large compressible flow problems, SPH should be improved. Especially, the calculation of pressure term is major issue.

1.2 Research Purpose

The objective of this study is to develop the whole process of underwater explosion only using SPH. The whole process of underwater explosion consists of shock wave propagation, bubble pulsation, and bubble jet. For the shock wave propagation, the phenomenon is present at early times with μs scale. Relatively, the phenomenon related to the bubble dynamics is late time effects with ms scale. Between the shock physics and the bubble dynamics, it also has different equation of state for pressure distribution. To deal with this problem, the numerical modules are implemented separately for each phenomenon. Therefore, a method to determine the point of converting from the shock physics to the bubble dynamics is required. For the bubble pulsation problem, Tait equation conventionally used to implement the multi-phase problem in SPH has difficulty in simulating the gas bubble pulsation phenomenon. Therefore, a new or modified state equation should be proposed in order to simulate the compression, expansion and the period of the gas bubble in accordance with the actual behavior. Finally, the verification of numerical model should be carried out through comparing with empirical formulations, other numerical method results, and experimental results.

Chapter 2. Methodology

2.1 Underwater Explosion Phenomena

2.1.1 Shock Wave

The shock wave propagation is one of the major phenomena of underwater explosion. It is generated after charge and propagates with high velocity. Increase in pressure causes the wave velocity to increase until the wave velocity exceeds the sound speed. Thus, the shock wave is found in the explosion. It has constant speed during propagation and the extremely high pressure.

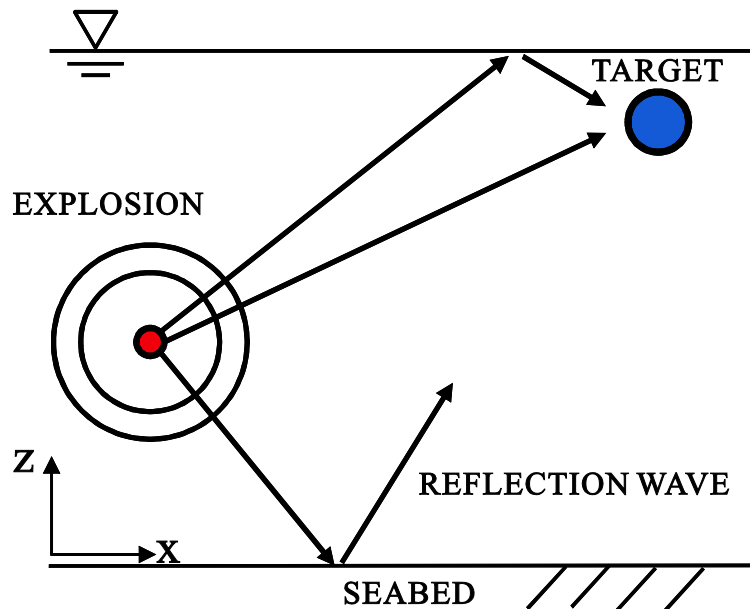


Figure 2.1. Shock wave propagation.

The shock wave induces the damage to the structure not only by directly hit, but also by reflection wave hit. It is shown in Fig. 2.1. The reflected wave is generated through reflecting from free surface or seabed. Especially, the reflection wave from free surface causes a surface cutoff phenomenon, which makes pressure drop around free surface. The pressure drop around free surface can induce bulk cavitation. On the contrary to this, the reflection wave from seabed propagates with high pressure similar to the direct wave propagation.

The explosion procedure generates heat with high temperature. However, in the case of the underwater

explosion, it can be diminished by surrounding water. Thus, heat transfer can be neglected.

2.1.2 Bubble Dynamics

After the underwater explosion, the bulk energy of an explosive is used to form the gas bubble with high temperature and pressure. The initial gas bubble pressure and maximum bubble radius can be calculated by the explosive type and quantity. The following empirical formulation is used for calculating it.

$$P_0 = K_1 \left(\frac{W}{V_0} \right)^{1.25} \quad (2.1)$$

$$R_{\max} = K_2 \left(\frac{W}{D + 10} \right)^{\frac{1}{3}} \quad (2.2)$$

Where K_1 , K_2 are coefficients for the explosive type, W is explosive weight and V_0 is initial charge volume. D is depth of the explosive point from free surface. By above equations, it can be known that the gas bubble has high temperature and pressure compared to surrounding water. Thus, the bubble expands and compresses repeatedly to reach state of equilibrium. During bubble pulsation, whenever reaching the maximum compressed state, pressure pulse is generated.

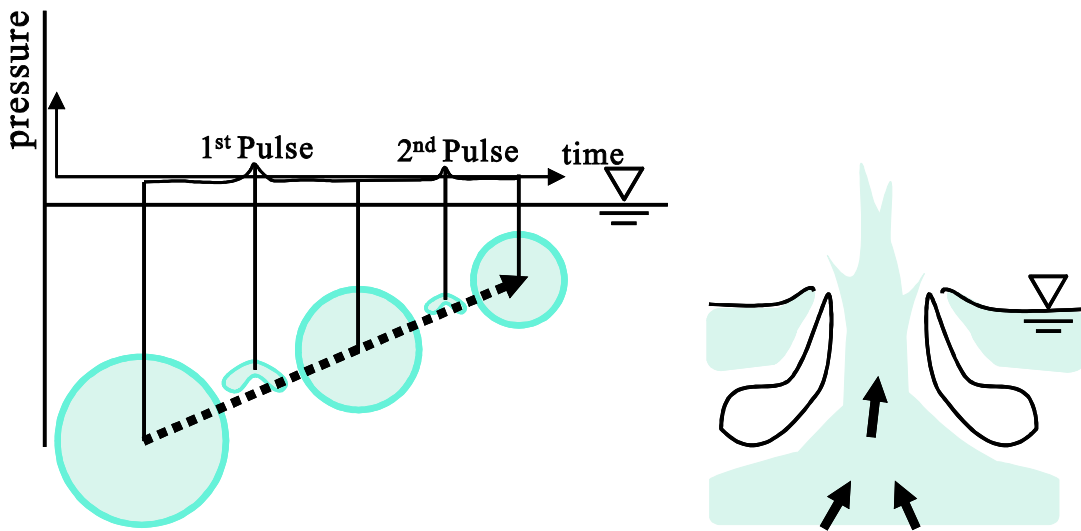


Figure 2.2. Behavior of bubble pulsation and bubble jet.

Initial gas bubble expansion occurs due to high pressure compared to the surrounding environment. Even after reaching equilibrium state of the pressure, it is continued by inertia. Thus, the gas bubble expansion lasts

until the internal pressure is lower than surrounding one. When reaching the maximum expansion state the gas bubble pressure is much lower than one of surrounding water. Consequentially, the gas bubble begins compression. That is, the pulsation motion is shown. Simultaneously, the drift behavior is started by buoyancy force.

As the gas bubble reaches free surface, the shape of bubble is transformed like a horseshoe. After the shape transforms into the horseshoe, the gas bubble is collapsed. During collapsing procedure, vortices are generated along with the horseshoe shape, and the empty place caused by the bubble collapsing is filled by surrounding fluid. That is, the water penetrates the gas bubble. The fluid flow like this is called bubble jet. Fig 2.2 shows the whole process of the bubble dynamics.

2.2 Formulation of SPH Method

In SPH method, there are 2 key steps to transform any field function to SPH formulation. The first step is *the integral representation*. The second one is *the particle approximation*. Using the 2 steps, any field function and its derivative function can be expressed appropriately for numerical analysis.

2.2.1 Integral Representation

In the integral representation step, the function of a given point can be expressed by integration of the multiplication of smoothing kernel function and the function of other points in the support domain of a given point. That is, the arbitrary function f is given by

$$\langle f(x) \rangle = \int_{\Omega} f(x')W(x-x',h)dx' \quad (2.3)$$

In SPH convention, angle bracket $\langle \rangle$ is usually used for marking the integral representation. Similarly, the integral representation of the derivative of a function can be derived by following procedure.

$$\langle \nabla \cdot f(x) \rangle = \int_{\Omega} [\nabla \cdot f(x')]W(x-x',h)dx' \quad (2.4)$$

Since

$$[\nabla \cdot f(x')]W(x-x',h) = \nabla \cdot [f(x')W(x-x',h)] - f(x') \cdot \nabla W(x-x',h) \quad (2.5)$$

From Equation(2.4), the following equation is obtained,

$$\langle \nabla \cdot f(x) \rangle = \int_{\Omega} \nabla \cdot [f(x')W(x-x',h)]dx' - \int_{\Omega} f(x') \cdot \nabla W(x-x',h)dx' \quad (2.6)$$

The first term on the right hand side of Equation(2.6) can be converted by divergence theorem.

$$\langle \nabla \cdot f(x) \rangle = \int_{\Omega} f(x')W(x-x',h)dx' - \int_{\Omega} f(x') \cdot \nabla W(x-x',h)dx' \quad (2.7)$$

By compact support condition of kernel function W , the first term on the right hand of Equation(2.7) should be zero. Therefore, Equation(2.7) can be simplified as follow.

$$\langle \nabla \cdot f(x) \rangle = - \int_{\Omega} f(x') \cdot \nabla W(x-x',h)dx' \quad (2.8)$$

By Equation(2.8), the derivative of a function is simply converted to a differential operation of kernel function.

2.2.2 Particle Approximation

In the 2nd step of SPH method, the whole system can be represented by the particle approximation. A finite number of particles have each physics values such as mass, velocity, and energy. The integral form from the integral representation can be transformed to the discretized form of summation concerning all the particles in the support domain. The following procedure in Equation(2.9) is to get the particle approximation form.

$$\begin{aligned} f(x) &= \int_{\Omega} f(x')W(x-x',h)dx' \\ &\cong \sum_{j=1}^N f(x_j)W(x-x_j,h)\Delta V_j \quad \text{where } m_j = \Delta V_j \rho_j \\ &= \sum_{j=1}^N f(x_j)W(x-x_j,h) \frac{1}{\rho_j} (\rho_j \Delta V_j) \\ &= \sum_{j=1}^N f(x_j)W(x-x_j,h) \frac{1}{\rho_j} (m_j) \end{aligned} \quad (2.9)$$

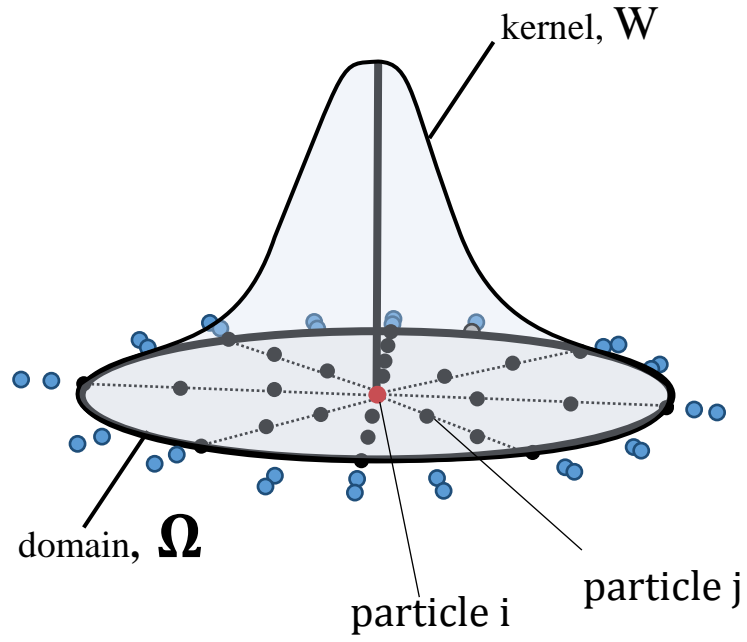


Figure 2.3. Kernel function model with support domain, Ω .

Fig. 2.3 shows that particle i is of interest and particle j is the neighbor particle, W is a kernel function in domain Ω . Using two key steps of SPH formulation, the arbitrary function and its derivative can be achieved as follow.

$$\langle f(x) \rangle = \sum_{j=1}^N \frac{m_j}{\rho_j} f(x_j) W(x - x_j, h) \quad (2.10)$$

$$\langle \nabla \cdot f(x) \rangle = - \sum_{j=1}^N \frac{m_j}{\rho_j} f(x_j) \cdot \nabla W(x - x_j, h) \quad (2.11)$$

2.2.3 Kernel Function

In SPH, the kernel function has some conditions. Firstly, the kernel function should be normalized and smoothed sufficiently.

$$\int_{\Omega} W(x - x', h) dx' = 1 \quad (2.12)$$

It also should have symmetrical form and compactly supported.

$$W(x - x') = 0, \text{ for } |x - x'| > \kappa h \quad (2.13)$$

As the smoothing length, h , approaches to zero, the kernel function should be the Dirac delta function.

$$\lim_{h \rightarrow 0} W(x - x', h) = \delta(x - x') \quad (2.14)$$

In the domain, it should be positive.

$$W(x - x') \geq 0 \quad (2.15)$$

Lastly, the function should be decaying with the increase of the distance away from the center of the domain.

There are several kernel functions as follows[10].

$$\text{Lucy (1977)} \quad W(x - x', h) = W(R, h) = \alpha_d \begin{cases} (1 + 3R)(1 - R)^3 & R \leq 1 \\ 0 & R > 1 \end{cases} \quad (2.16)$$

$$\text{Monaghan (1985)} \quad W(R, h) = \alpha_d \left(\frac{3}{2} - R^2 \right) e^{-R^2} \quad 0 \leq R \leq 2 \quad (2.17)$$

$$\text{Moris (1994)} \quad W(R, h) = \alpha_d \begin{cases} (R + 2.5)^4 - 5(R + 1.5)^4 + 10(R + 0.5)^4 & 0 \leq R < 0.5 \\ (2.5 - R)^4 - 5(1.5 - R)^4 & 0.5 \leq R < 1.5 \\ (2.5 - R)^4 & 1.5 \leq R < 2.5 \\ 0 & R > 2.5 \end{cases} \quad (2.18)$$

$$\text{Moris (1996)} \quad W(R, h) = \frac{1}{\pi h^2} \left[\frac{e^{-(R/h)^2} - e^{-9}}{1 - 10e^{-9}} \right] \quad R \leq 3h \quad (2.19)$$

In this study, the renormalized Gaussian kernel function(Moris 1996) is adopted due to the better stability properties.

2.3 Numerical Approximation

2.3.1 Governing Equation

For general flow, the physics phenomena are governed by the Navier-Stokes equations which are derived from the Newton's law for mass and momentum. It is shown as follow.

$$\left\{ \begin{array}{l} \frac{D\rho}{Dt} = -\rho \frac{\partial v^\beta}{\partial x^\beta} \\ \frac{Dv^\alpha}{Dt} = \frac{1}{\rho} \frac{\partial \sigma^{\alpha\beta}}{\partial x^\beta} \quad \text{where } \sigma^{\alpha\beta} = -p\delta^{\alpha\beta} + \tau^{\alpha\beta} \\ \frac{De}{Dt} = \frac{\sigma^{\alpha\beta}}{\rho} \frac{\partial v^\alpha}{\partial x^\beta} \end{array} \right. \quad (2.20)$$

Where ρ, v, e, t are density, velocity vector, internal energy, and time respectively. σ is the total stress tensor consists of pressure part(p) and viscous stress part (τ). Above governing equation can be converted to SPH formulation form as follow.

$$\left\{ \begin{array}{l} \frac{D\rho}{Dt} = -\rho \frac{\partial v^\beta}{\partial x^\beta} \cong \rho_i \sum_{j=1}^N \frac{m_j v_{ij}^\beta}{\rho_j} \frac{\partial W_{ij}}{\partial x_i^\beta} \\ \frac{Dv^\alpha}{Dt} = \frac{1}{\rho} \frac{\partial \sigma^{\alpha\beta}}{\partial x^\beta} \cong \sum_{j=1}^N m_j \frac{\sigma_i^{\alpha\beta} + \sigma_j^{\alpha\beta}}{\rho_i \rho_j} \frac{\partial W_{ij}}{\partial x_i^\beta} \quad \text{where } \sigma^{\alpha\beta} = -p\delta^{\alpha\beta} + \tau^{\alpha\beta} \\ \frac{De}{Dt} = \frac{\sigma^{\alpha\beta}}{\rho} \frac{\partial v^\alpha}{\partial x^\beta} \cong \frac{1}{2} \sum_{j=1}^N m_j \left(\frac{p_i + p_j}{\rho_i \rho_j} \right) v_{ij}^\beta \frac{\partial W_{ij}}{\partial x_i^\beta} + \frac{\mu_i}{2\rho_i} \varepsilon_i^{\alpha\beta} \varepsilon_i^{\alpha\beta} \end{array} \right. \quad (2.21)$$

To simulate the shock wave propagation and two phase flow, above standard SPH formulation has a few limitations. At the interface, the presence of a sharp density gradient induces severe numerical instability. The volume approximation method which is proposed by Hu and Adams[7] is adopted to solve this problem. By the summation density equation as follow,

$$\rho_i = m_i \sum_{j=1}^N W(x_i - x_j, h) \quad (2.22)$$

The volume approximation is derived.

$$\rho_i = m_i \sum_{j=1}^N W(x_i - x_j, h) = \frac{m_i}{V_i} \quad (2.23)$$

$$V_i = \frac{1}{\sum_{j=1}^N W(x_i - x_j, h)} \quad (2.24)$$

Using this relation, the governing equation can be converted as follow.

$$\left\{ \begin{array}{l} \rho_i = m_i \sum_{j=1}^N W_{ij} \\ \frac{Dv_i^\alpha}{Dt} = \frac{1}{\rho_i} \left(-\frac{1}{V_i} \sum_{j=1}^N (\sigma_i^{\alpha\beta} V_i^2 + \sigma_j^{\alpha\beta} V_j^2) \frac{\partial W_{ij}}{\partial x_i^\beta} \right) \quad \text{where } \sigma^{\alpha\beta} = -p\delta^{\alpha\beta} + \tau^{\alpha\beta} \\ \frac{De}{Dt} = \frac{1}{2\rho_i} \left(\frac{1}{V_i} \sum_{j=1}^N (\sigma_i^{\alpha\beta} V_i^2 + \sigma_j^{\alpha\beta} V_j^2) v_{ij}^\beta \frac{\partial W_{ij}}{\partial x_i^\alpha} \right) + \frac{\mu_i}{2\rho_i} \varepsilon_i^{\alpha\beta} \varepsilon_i^{\alpha\beta} \end{array} \right. \quad (2.25)$$

2.3.2 Viscosity

For problems of hydrodynamics, the influence of viscosity is directly related to the accuracy of the numerical result. By SPH researchers several kinds of methods to express the viscosity are suggested. The mainly used viscous equation is the formulation proposed by Monaghan[17].

$$F_{Monaghan}(x_i) = \sum_{j=1}^N \Pi_{ij} \nabla W_{ij} \frac{m_j}{\rho_j} \quad (2.26)$$

$$\Pi_{ij} = \frac{-\alpha_\Pi \bar{c}_{ij} \phi_{ij} + \beta_\Pi \phi_{ij}^2}{\bar{\rho}_{ij}} \quad (2.27)$$

$$\phi_{ij} = \frac{h_{ij} \mathbf{u}_{ij} \cdot \mathbf{x}_{ij}}{|\mathbf{x}_{ij}|^2 + (\varepsilon h_{ij})^2} \quad (2.28)$$

In the shock physics simulation, to prevent particle penetration the coefficient α_Π is set to 1 and β_Π is set to about 10. The factor ε is set mainly from 0.01 to 0.1 for preventing the denominator vanishing.

In the simulation of multiphase problem, several other methods for the viscosity are more stable than Monaghan. As one of them, Hu and Adams presented a new formulation for the multiphase problem as follow[7].

$$F_{Hu}(x_i) = \sum_{j=1}^N \frac{2\eta_i \eta_j}{(\eta_i + \eta_j)} (V_i^2 + V_j^2) \frac{\mathbf{x}_{ij} \cdot \nabla W_{ij}}{x_{ij}^2 + (\varepsilon h_{ij})^2} \frac{\mathbf{u}_{ij}}{V_i} \quad (2.29)$$

Where η is dynamic viscosity, V is volume of a particle and ε is usually set to 0.01, u is velocity. Equation(2.29) has the form based on the volume approximation. In this study, Monaghan formulation is used for the shock physics simulation while the formulation proposed by Hu and Adams is used for the bubble dynamics simulation.

2.4 SPH Implementation

2.4.1 Tree-Search Algorithm

To find neighboring particles, a specific algorithm is needed. The simplest way is Direct find method. Direct find method is to check whether the interaction is valid or not about total particles. It is carried out for every i particles, and the searching is also performed for all j particles. Therefore, the computational cost has order $O(N^2)$. The searching process like this should be performed at all the time steps, the computational cost for Direct find method is too expensive. In this paper, Tree-Search algorithm is used for problems of large scale.

Tree-Search algorithm is divided into two stages. The first one is construction of tree structure and the second one is searching process.

The maximum problem domain is split into quadrants for 2-dimensional problems or octants for 3-dimensional problems. It happens recursively until each partitioned domain has only one particle(Figure 2.4).

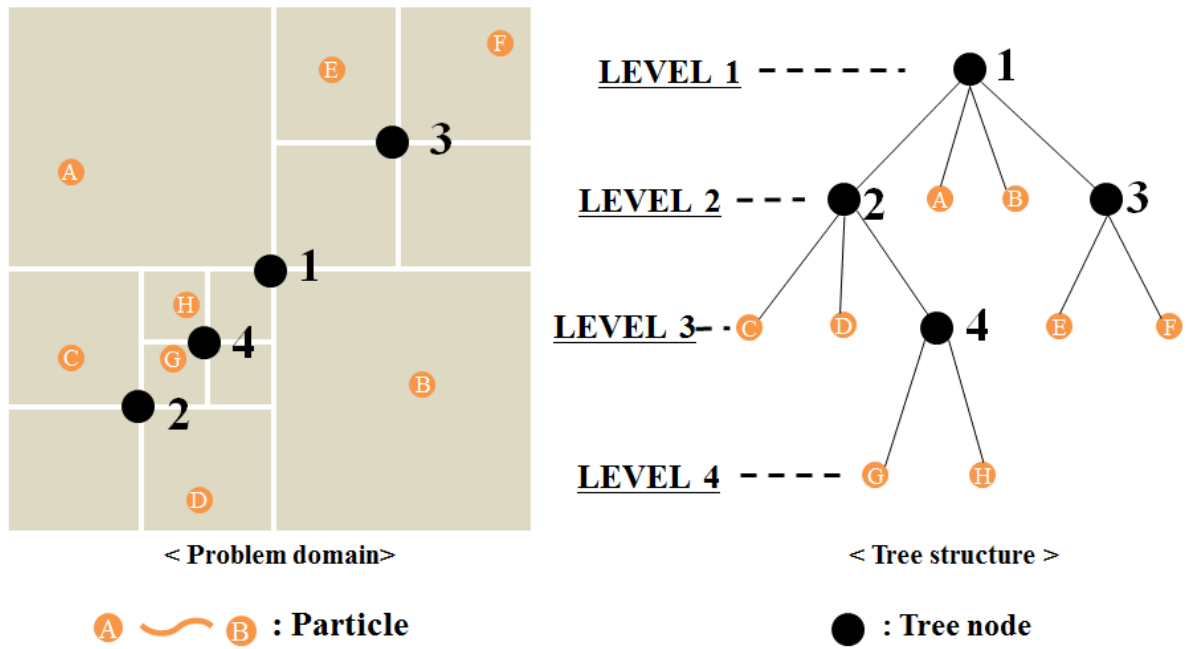


Figure 2.4. Tree structure about whole domain.

Searching process is proceeded as follow. For a given particle i , it has a cube with the side of the length larger than smoothing length, which has the center on the particle i . There are some tree nodes which have each volume. The cube of particle i is checked whether the cube area overlaps each node volume at each level. If the cube area overlaps the tree node volume, continue the descent down to the next level until the node only represents a particle. Whenever the node represents a particle, it is checked to whether the particle is within the support domain of particle i or not. This algorithm is of order $O(N \log N)$. Table 2.1 shows the result of comparing the computational cost of Direct find method and Tree-Search algorithm.

Table 2.1. Computational cost comparison of between searching algorithms.

The number of particle	Algorithm				Ratio
	Direct Find algorithm		Tree Search algorithm		
	1 step	100 step	1 step	100 step	
14400	2.7~3.0(s)	299.77(s)	0.10~0.15(s)	19.67(s)	0.0656
90000	95~115(s)	10443.73(s)	0.85~0.95(s)	113.9(s)	0.0109

For 14400 particles, the computational cost of Direct find method is 15 times higher than Tree-Search algorithm. For 90000 particles, Tree-Search algorithm is 92 times faster than Direct find method.

2.4.2 Boundary Conditions

In SPH, there are some methods to impose boundary conditions. Monaghan used virtual particles on the solid boundary which apply repulsive force to the particles approaching the boundary. The repulsive force is used to prevent the particles located in domain from penetrating the boundary. The following formulation is presented[10].

$$RF_{ij} = D \left[\left(\frac{r_0}{r_{ij}} \right)^{n_1} - \left(\frac{r_0}{r_{ij}} \right)^{n_2} \right] \frac{x_{ij}}{r_{ij}^2} \quad \left(\frac{r_0}{r_{ij}} \leq 1 \right) \quad (2.30)$$

Where D is problem dependent parameter, and is proposed as square of 5gH or 10gH which is the same scale with the largest velocity. r_0 is set to the initial particle distance, n_1, n_2 are usually chosen as 12 and 4 respectively. The above formulation can induce numerical instability when particles approach to the boundary so closely.

Other boundary treatment scheme is using mirror particle[10]. The mirror particle has same properties with the real particle like density, mass, energy, pressure, smoothing length. But for position and velocity it is applied differently. For example, at the left boundary, the velocity value of the x direction is opposite to the real particle while the y direction velocity value is same with the real particle. For the lower boundary, the x direction velocity value coincides with the real particle while the y axis velocity value is opposite direction of the thing of the real particle. For position, the mirror particle has the position of boundary axisymmetric about the real particle. Following formulation is a simple case of the mirror particle position and velocity for 2-dimensional case.

The position of the mirror particle

$$\left\{ \begin{array}{l} \text{At the left boundary : } x_{mirror} = -x_{real}, y_{mirror} = y_{real} \\ \text{At the right boundary : } x_{mirror} = 2x_{boundary} - x_{real}, y_{mirror} = y_{real} \\ \text{At the lower boundary : } y_{mirror} = -y_{real}, x_{mirror} = x_{real} \\ \text{At the upper boundary : } y_{mirror} = 2y_{boundary} - y_{real}, x_{mirror} = x_{real} \end{array} \right. \quad (2.31)$$

The velocity of the mirror particle

$$\left\{ \begin{array}{l} \text{At the left boundary : } u_{mirror} = -u_{real}, v_{mirror} = v_{real} \\ \text{At the right boundary : } u_{mirror} = -u_{real}, v_{mirror} = v_{real} \\ \text{At the lower boundary : } v_{mirror} = -v_{real}, u_{mirror} = u_{real} \\ \text{At the upper boundary : } v_{mirror} = -v_{real}, u_{mirror} = u_{real} \end{array} \right. \quad (2.32)$$

In this study, we use the mirror particle for almost cases because the numerical instability of virtual particle mentioned above. A free slip boundary condition as Equation(2.31,2.32) is applied for all our simulation cases.

2.4.3 Interface Sharpness Treatment

For the multiphase problem, the interface sharpness treatment is a significant factor for the behavior of the simulation. To keep the interface smoothed, when the other type's particles interact with each other, the proper force is applied to each particle. This concept is presented by Colagrossi[1] firstly, since then, some researchers like Grenier et al.[4] has developed the method. The force is called the interface sharpness force, acts like a repulsive force perpendicular to the interface. However, if the force is too bigger, it breaks the physics behavior. So then, in this study the force multiplied by the coefficient 0.08 is introduced. The formulation is as follow.

$$F_{ISF}(x_i) = -\frac{0.08}{\rho_i V_i} \sum_{j=1}^N (|p_i| V_i^2 + |p_j| V_j^2) \nabla_i W_{ij} \quad (2.33)$$

2.4.4 Time Integration Scheme

In the SPH research field, the explicit time integration scheme is used for updating the governing equation as time progress. Of them, Reap-frog, Runge-Kutta, Predictor-corrector schemes are mainly adopted. In this

study, the modified predictor-corrector scheme is applied due to the numerical stability and the computational cost. The scheme is presented by Zhang[24] and is motivated to control the pressure oscillation caused by the interface sharpness force. The difference from the existing scheme is that position updating is determined by the recently updated velocity. The formulation is as follows.

$$\text{Prediction step} \quad \left\{ \begin{array}{l} \rho_i^{(n+1)/2} = m_i \sum_j^N (W_{ij})^n \\ u_i^{(n+1)/2} = u_i^n + \frac{\Delta t}{2} \left(\frac{Du}{Dt} \right)_i^n \\ r_i^{(n+1)/2} = r_i^n + \frac{\Delta t}{2} u_i^{(n+1)/2} \end{array} \right. \quad (2.34)$$

$$\text{Correction step} \quad \left\{ \begin{array}{l} \rho_i^{(n+1)} = m_i \sum_j^N (W_{ij})^{(n+1)/2} \\ u_i^{(n+1)} = u_i^n + \Delta t \left(\frac{Du}{Dt} \right)_i^{(n+1)/2} \\ r_i^{(n+1)} = r_i^n + \Delta t u_i^{(n+1)} \end{array} \right. \quad (2.35)$$

The interval of the time step Δt is assigned dynamically considering CFL condition which is used in the conventional SPH research field. In this case, in the aspect of the numerical stability and the computational cost it can be used more effectively than the static time step.

$$\Delta t = \min\left(0.125 \frac{\rho h^2}{\eta}, 1.0 \frac{h}{c + u_{\max}}\right) \quad (2.36)$$

2.5 Equation of State for Pressure

In SPH, the pressure term is explicitly calculated by some equations of state. The equation of state for pressure is employed differently for each physical phenomenon. It is a very significant factor that affects both the numerical stability and the computational cost. By choosing the equation properly, the SPH represents compressible fluid or incompressible fluid.

2.5.1 Pressure Equation for Shock Physics

For shock wave propagation, the standard Jones-Wilkins-Lee(JWL) equation is used for pressure of the explosive gas.

$$p = A\left(1 - \frac{\omega\eta}{R_1}\right)e^{-\frac{R_1}{\eta}} + B\left(1 - \frac{\omega\eta}{R_2}\right)e^{-\frac{R_2}{\eta}} + \omega\eta\rho_0 E \quad (2.37)$$

Where A, B, R_1, R_2, ω are coefficients concerning the state of the explosive.

η is the ratio of initial density to explosive density, $\eta = \rho / \rho_0$

Mie-Gruneisen state equation is employed for water in the shock wave simulation.

$$\mu > 0 \quad p = \frac{\rho_0 C^2 \mu [1 + (1 - \frac{\gamma_0}{2})\mu - \frac{a}{2}\mu^2]}{[1 - (S_1 - 1)\mu - S_2 \frac{\mu^2}{\mu + 1} - S_3 \frac{\mu^3}{(\mu + 1)^2}]^2} + (\gamma_0 + a\mu)E \quad (2.38)$$

$$\mu < 0 \quad p = \rho_0 C_0^2 \mu + (\gamma_0 + a\mu)E \quad (2.39)$$

Where μ is the ratio of compression, when water is in compressed state, $\mu > 0$, for expanded state, $\mu < 0$. C is velocity of sound; E is internal energy; ρ_0 is the initial density; $\gamma_0, a, S_1, S_2, S_3$ are fitting coefficient.

2.5.2 Pressure Equation for Bubble Dynamics

For bubble dynamics simulation, the following state of equation called Tait equation is employed for the gas bubble.

$$p = P_0 \left[\left(\frac{\rho}{\rho_0} \right)^\gamma - 1 \right] \quad (2.40)$$

Where coefficients P_0, γ are chosen to have density oscillations bounded in 1% concerning initial density ρ_0 . Generally, the initial pressure P_0 is derived by multiplying sound speed and initial density.

$$P_0 = \frac{C^2 \rho_0}{\gamma} \quad (2.41)$$

In this paper, the modified Tait equation is suggested for water. Two additional terms is added to the basic

Tait equation. The first one is pressure term for atmosphere and the second is for hydrostatic. These additional terms don't affect behavior of the simulation but influence the simulation period. Except for these additional terms, the bubble pulsation period is about 10 times longer than the real physics phenomenon.

$$P_{water} = P_0 \left[\left(\frac{\rho}{\rho_0} \right)^\gamma - 1 \right] + P_{atm} + P_{hyd} \quad (2.42)$$

2.6 Transition Point

The numerical scheme of underwater explosion procedure is divided into two parts on a bigger scale. The one is the shock physics part and the other one is the bubble dynamics part (Figure 2.5). The shock physics part employs the JWL equation and Mie-Gruneison state equation for calculating pressure while the bubble dynamics part uses the Tait equation and the modified Tait equation presented in this study. In addition, each physics simulation has the different time scale. The shock physics simulation has μs time scale while ms time scale is shown for the bubble dynamics simulation. That is why two separate numerical modules are needed. Also, for the connection of the two modules, a specific method for obtaining the transition point is required.

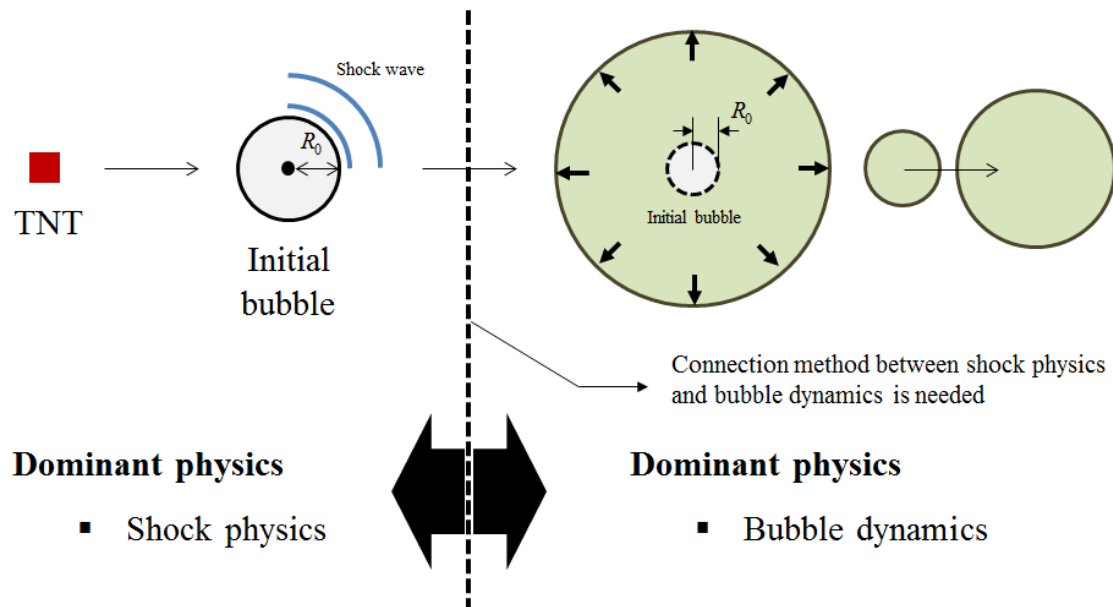


Figure 2.5. Classification of each physical phenomenon.

In this study, the transition point using the empirical formulation, Equation (2.1), is suggested. At first, the shock physics simulation is progressed. During the process, the gas bubble radius and pressure value is attained at each time step. The gas bubble radius calculated by numerical analysis is used as input value of Equation(2.1). Consequentially, the pressure value from empirical formulation is obtained using the numerical gas bubble radius. At every time step, a relative error between the numerical pressure value and the empirical pressure value is calculated. If the error is smaller than 0.5 %(0.005), the simulation module is transformed from the shock physics to the bubble dynamics. The pressure value and radius at the transition point is utilized as input value of the bubble dynamics simulation. The flow chart is showed in Figure 2.6.

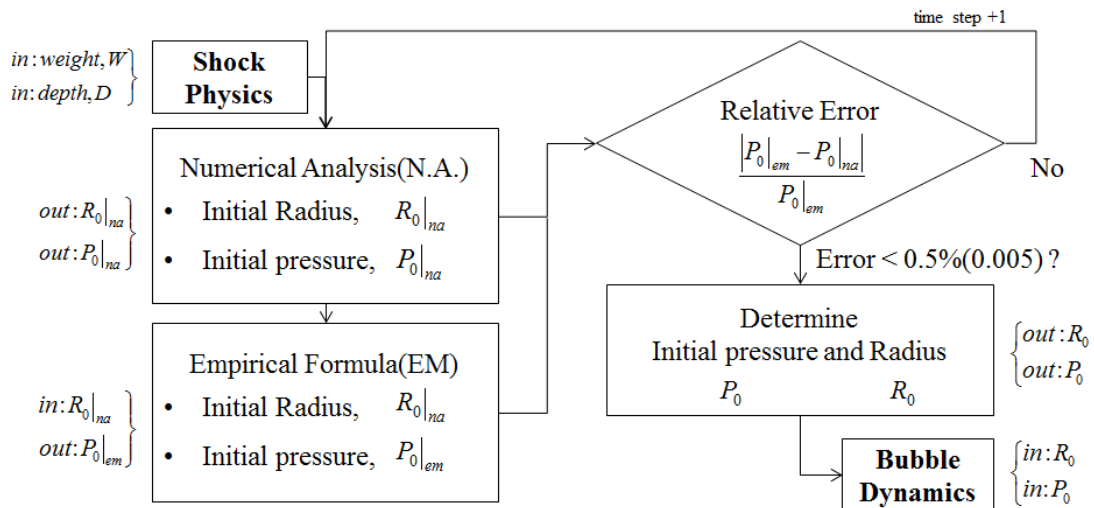


Figure 2.6. Flow chart for describing a method for obtaining the transition point.

In SPH, there is a crucial limitation to simulate expansion of the gas bubble. The high pressure gas bubble particles penetrate the surrounding water particles with relatively low pressure. In case that the interface treatment force is applied to prevent the phenomenon, the gas bubble behavior is to be unphysical by too large reaction force. The other method is that high sound speed as input value of the Tait state equation is considered. It causes the incompressibility of the surrounding water to be higher. However, this way induces the numerical instability and also has a negative impact on the overall simulation behavior.

As an alternative, after omitting the initial expansion stage, the state with maximum bubble size is considered as the start point of the bubble pulsation simulation. The maximum radius can be obtained by the empirical formulation in Equation (2.2) if knowing explosive weight and depth of explosion, or can be calculated by Rayleigh-Plesset equation in Equation (2.44). For pressure value of the maximal expansion bubble, it can be calculated by adiabatic gas law in Equation (2.43) that requires the pressure value and radius of the initial bubble, and the radius of maximal bubble as input value.

$$p = P_0 \left(\frac{R_0}{R} \right)^{3.75} \quad (2.43)$$

$$\frac{P_B - P_{ref}}{\rho} = R \frac{d^2 R}{dt^2} + \frac{3}{2} \left(\frac{dR}{dt} \right)^2 + \frac{4\mu}{\rho R} \frac{dR}{dt} + \frac{2\sigma}{\rho R} \quad (2.44)$$

The pressure value obtained from the above procedure is used for P_0 of the Tait equation. Consequently, the state equation for gas is as follow.

$$p_{gas} = P_0|_{cm} \left(\frac{R_0|_{cm}}{R_{max}} \right)^{3.75} \left[\left(\frac{\rho}{\rho_0} \right)^\gamma - 1 \right] \quad (2.45)$$

Where $P_0|_{cm}$, $R_0|_{cm}$ are the values attained from the transition point.

Chapter 3. Numerical Results

3.1 Dam Breaking Simulation

The dam breaking simulation used as a basic validation model of SPH is carried out. The dam breaking simulation is a simulation that observes the collapse of a certain amount of water column by gravity. The numerical model of this simulation is as follow.

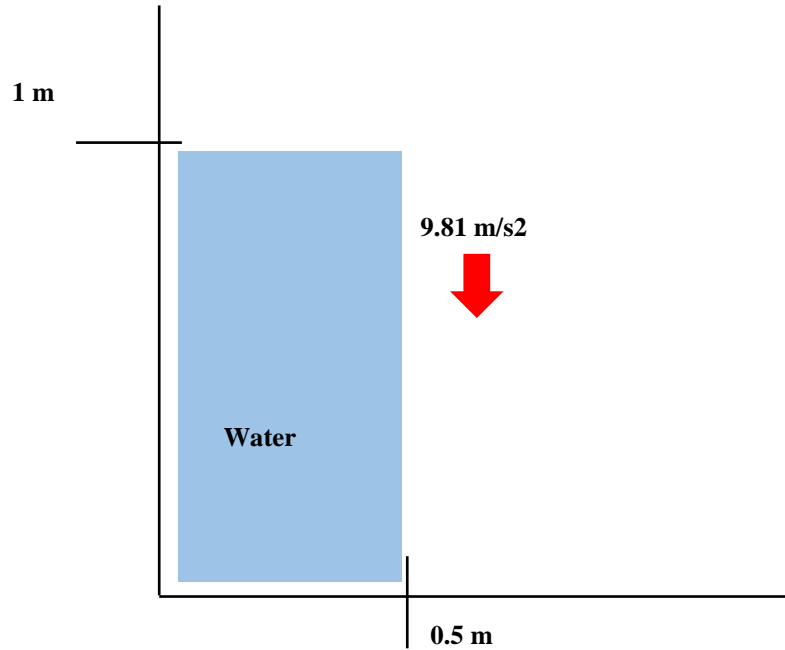


Figure 3.1. Numerical model of dam breaking simulation.

The simulation is performed by applying a gravitational acceleration of 9.81 m/s^2 to a water column having a density of 1000 kg/m^3 with a height of 1.0 m and a width of 0.5 m . 800 particles and 1800 particles are used for the simulation and the results are compared with experimental result of existing study.

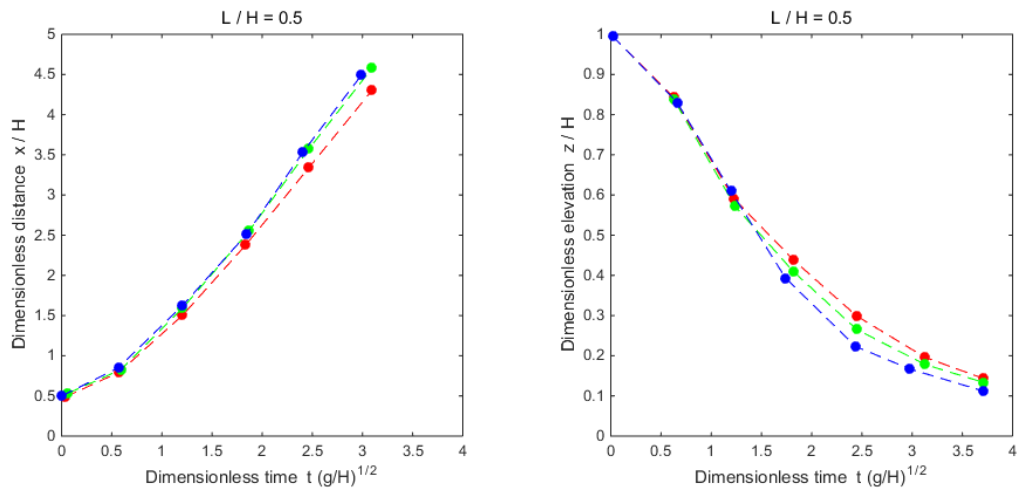


Figure 3.2. Comparison of a experiment and SPH. Left : progression of water over time. Right : Elevation of water column over time. Blue dot : experimental result. Green dot : SPH result of 1800 particles. Red dot : SPH result of 800 particles.

The x-axis on the two graphs in Figure 3.2 is the time. The y-axis of the left graph means the horizontal progress distance of water while the y-axis of the right graph shows the change in elevation of the water column. The red line means the 800 particles simulation and the green line shows the 1800 particles simulation while the blue line represents the experimental result. It can be seen that it becomes closer to the experiment as the number of particles increases.

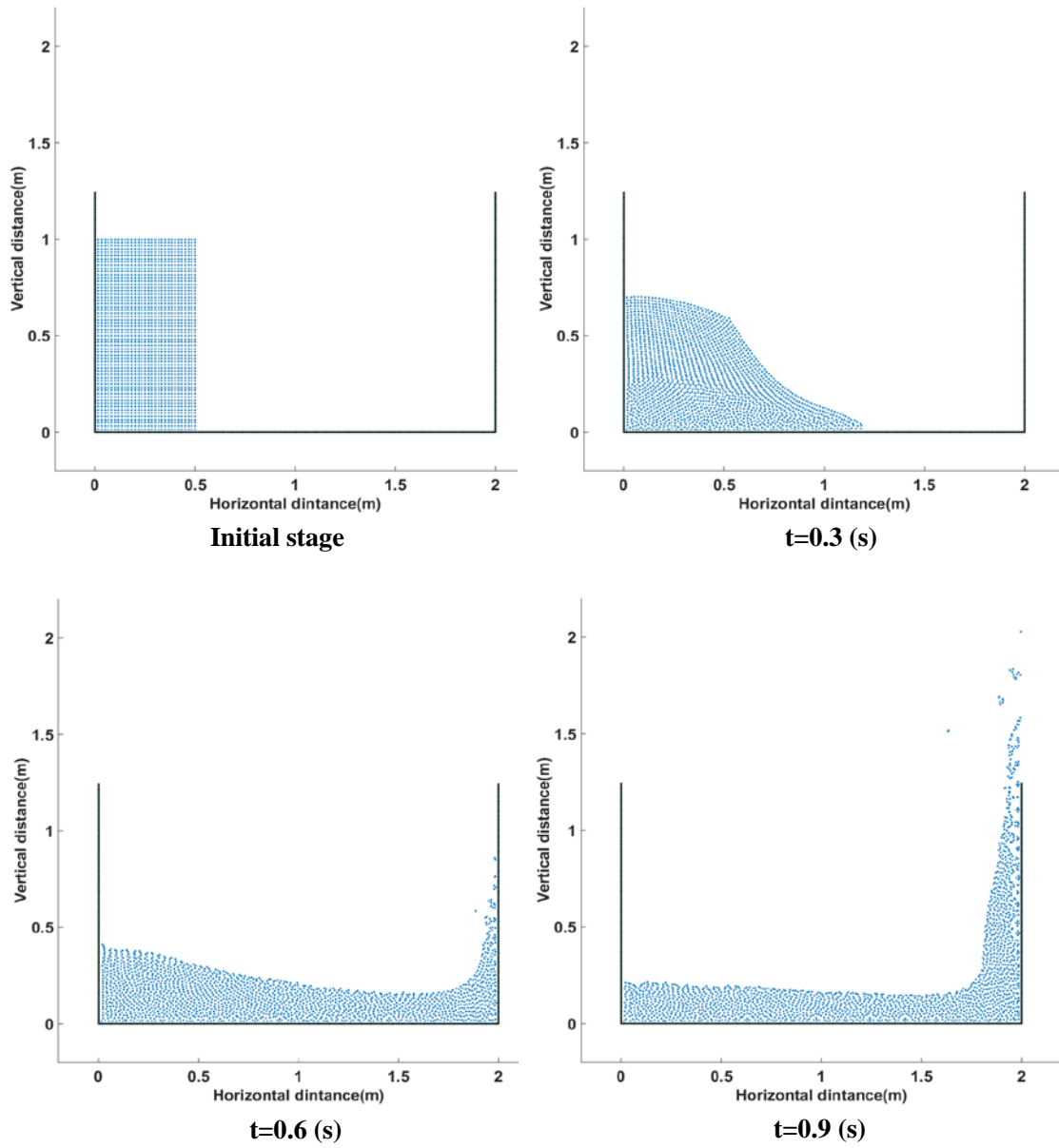


Figure 3.3. Dam breaking simulation from initial stage to 0.9 s.

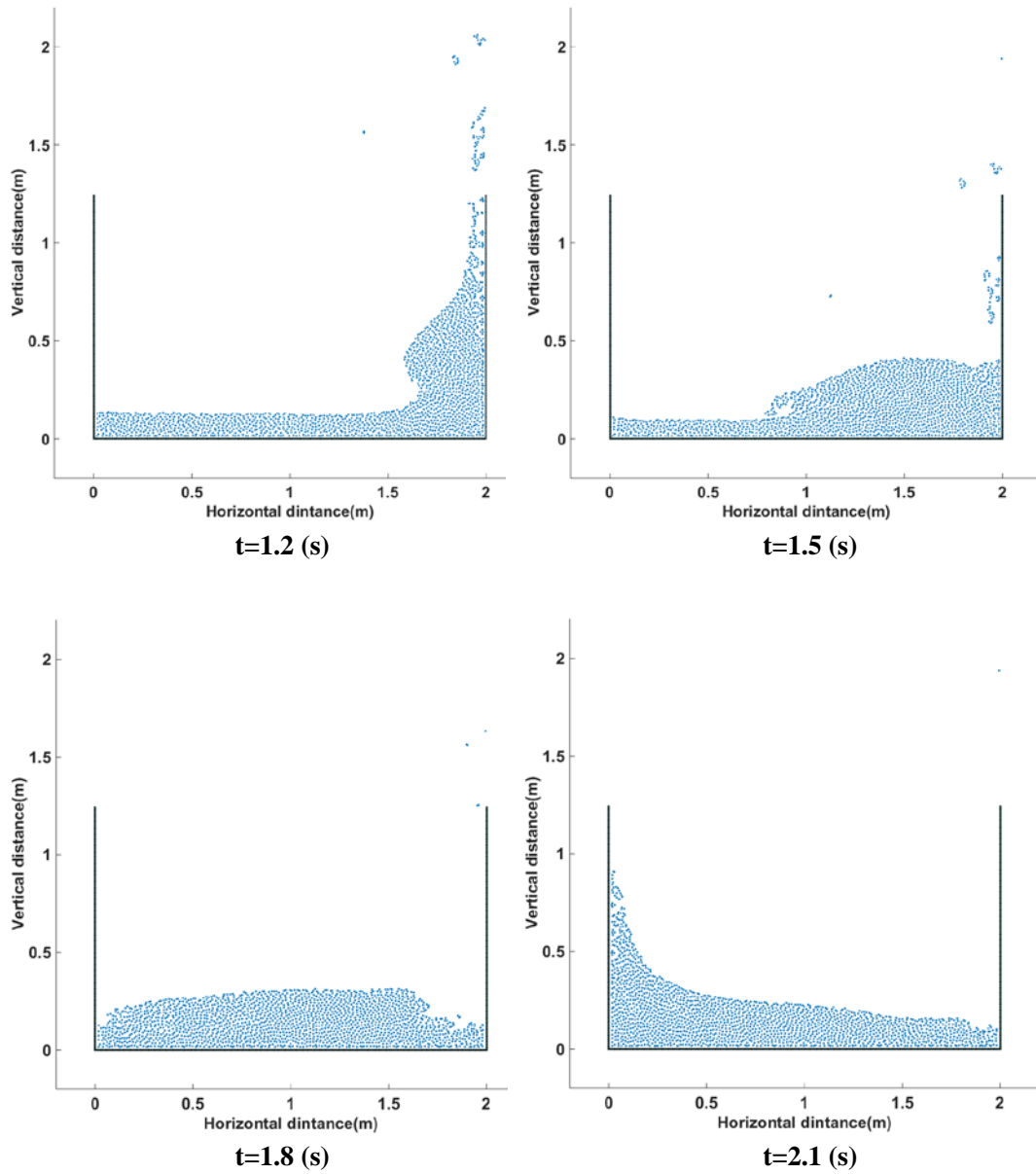


Figure 3.4. Dam breaking simulation from 1.2 s to 2.1 s.

3.2 Shock Wave Simulation

In the case of the shock wave simulation, the simulation is performed using the Jones-Willkins-Lee equation and the Mie-Gruneison equation. By the Mie-Gruneison equation, a compressed fluid has a high pressure, and the shockwave simulation is described via the propagation of this compressibility. The numerical model is as Figure 3.5.

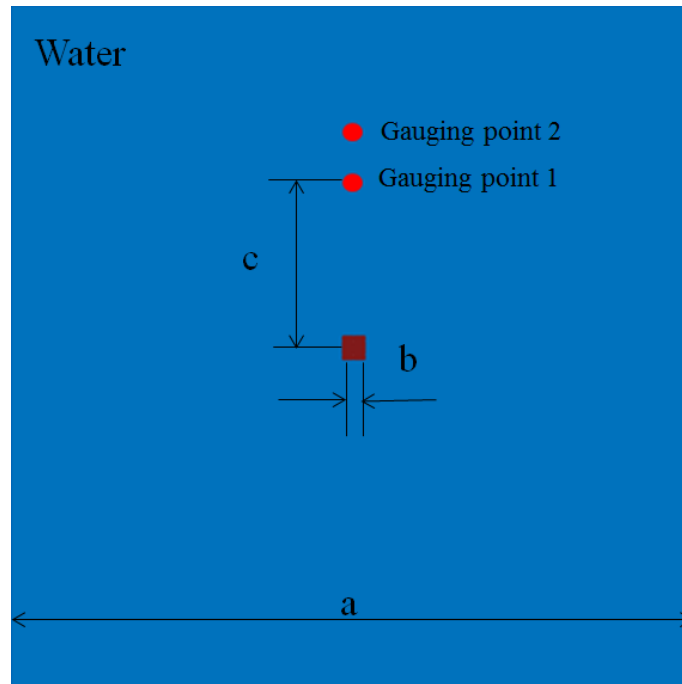


Figure 3.5. Numerical model of free field shock wave simulation.

Square TNT is used as explosive, $a = 3.0$ m, $b = 0.1$ m. Gauging point 1 and 2 are located at $c = 0.72$ m, 0.94 m respectively. The total number of particles used in the shock wave simulation is 90000 particles. The number of the water particle is 89900 while the gas particle is 100. The empirical formulation presented by Zamyshlyayev[23] is used for validation.

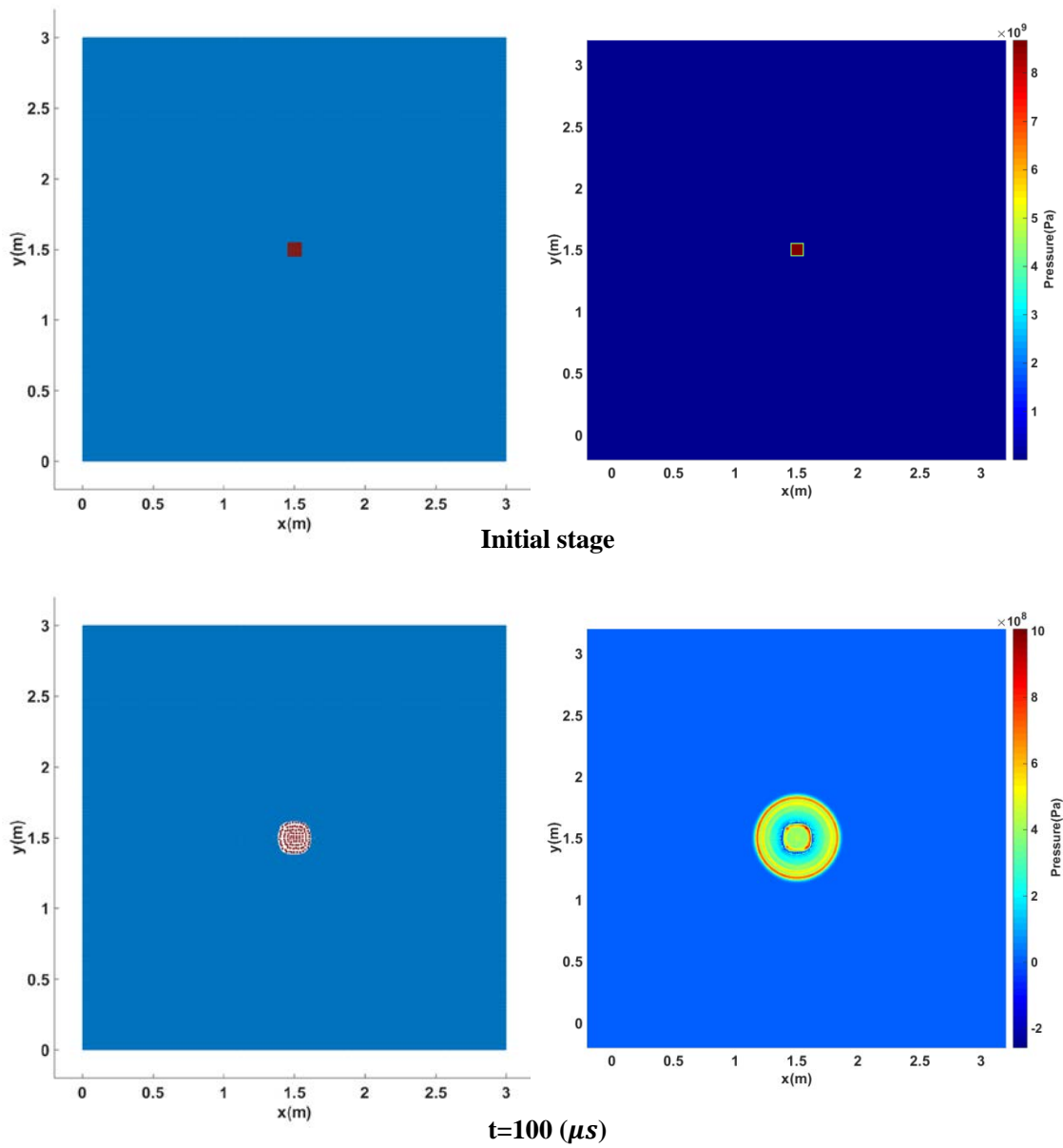


Figure 3.6. Shock wave simulation from initial stage to 100 μs . Left : particle behavior. Right : pressure distribution.

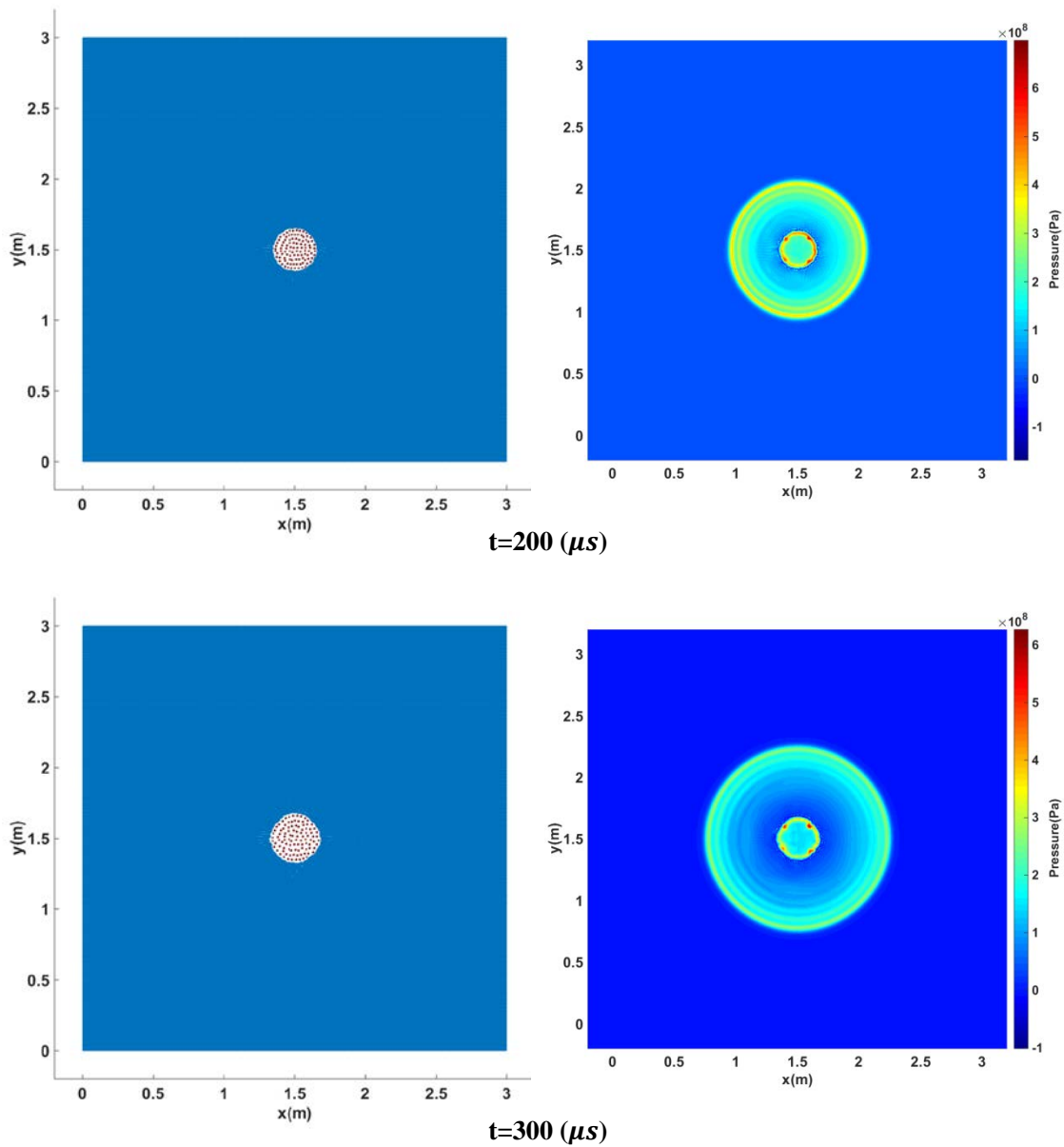


Figure 3.7. Shock wave simulation from $200 \mu\text{s}$ to $300 \mu\text{s}$. Left : particle behavior. Right : pressure distribution.

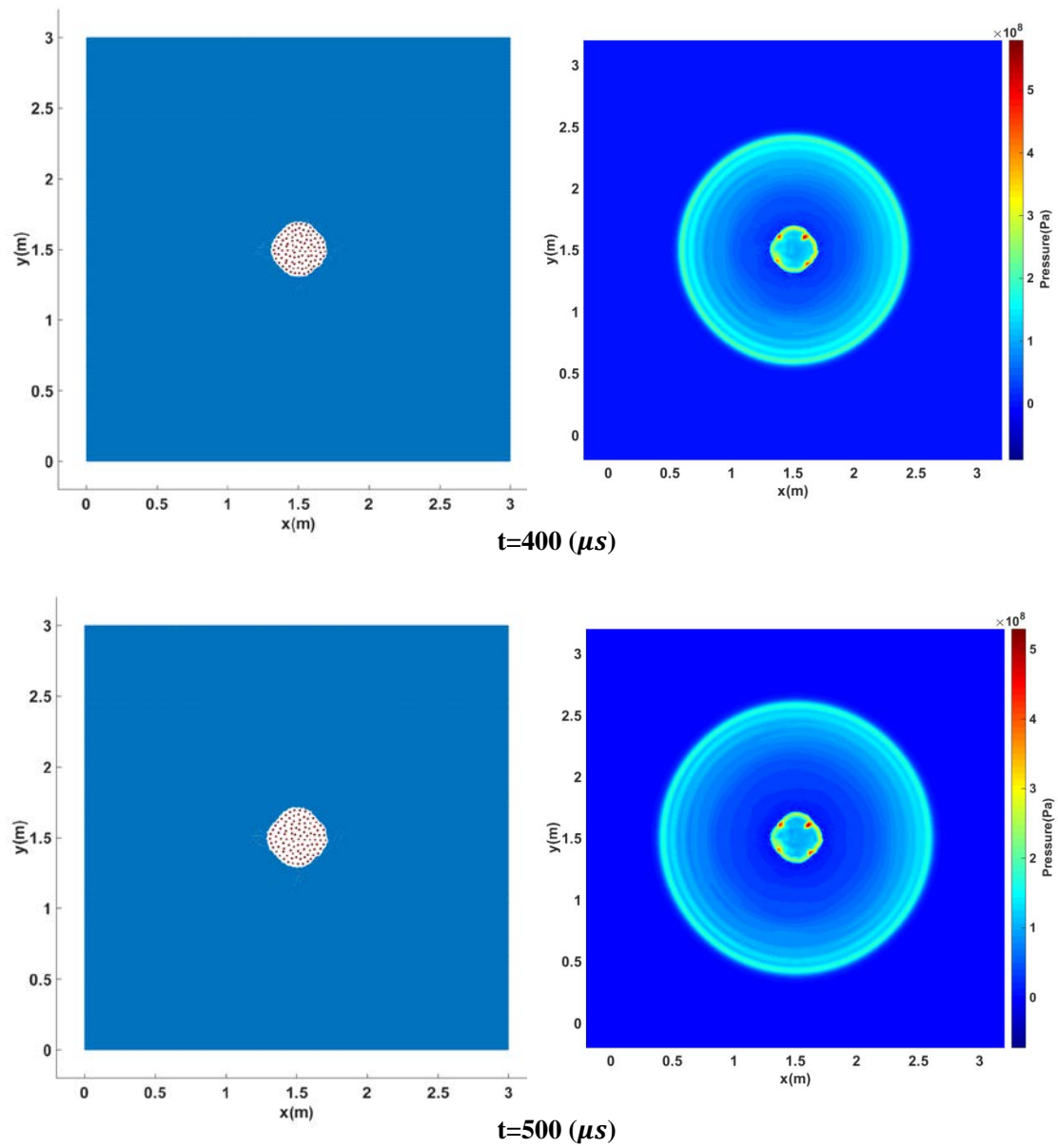


Figure 3.8. Shock wave simulation from $400 \mu\text{s}$ to $500 \mu\text{s}$. Left : particle behavior. Right : pressure distribution.

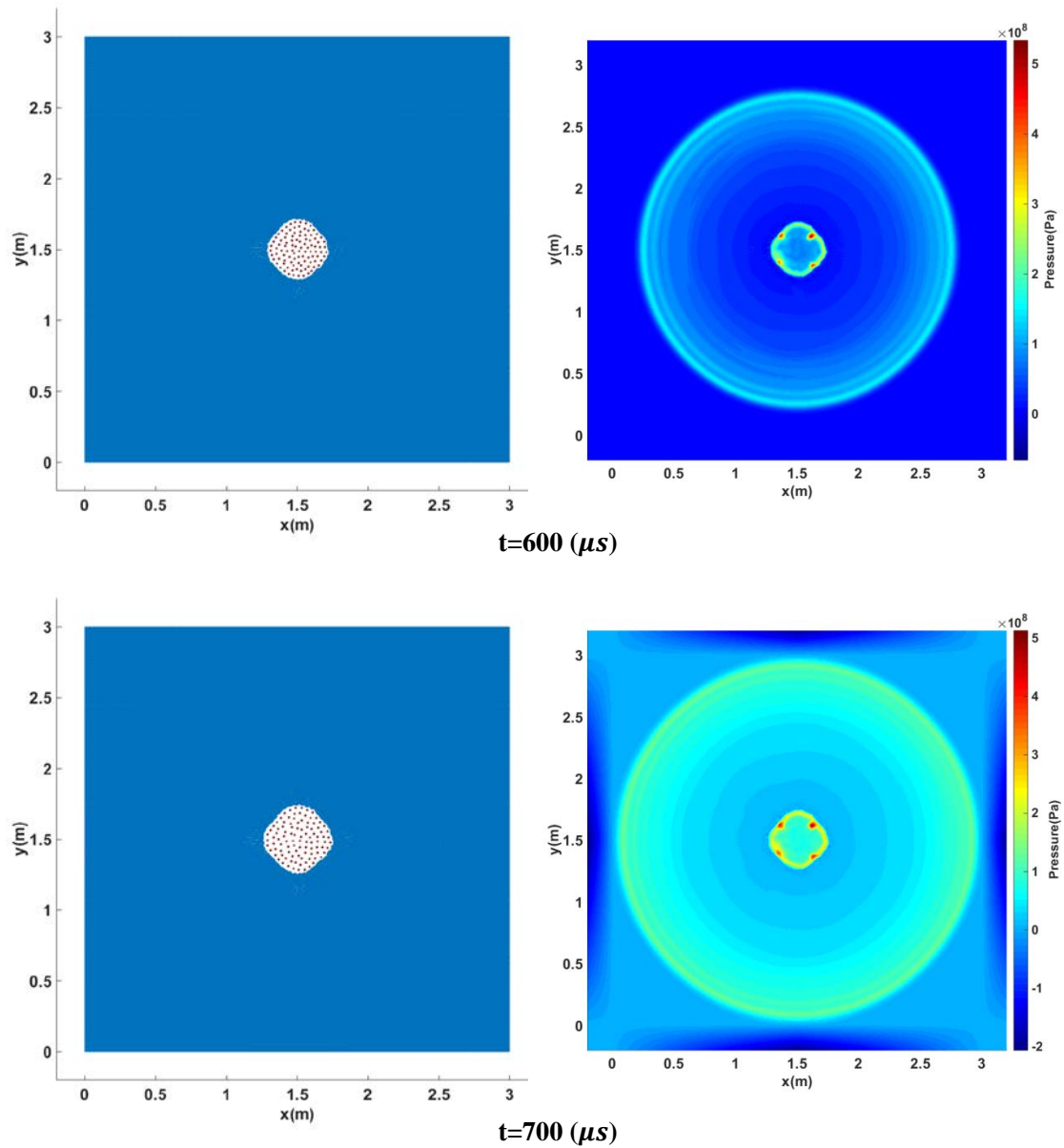


Figure 3.9. Shock wave simulation from $600 \mu s$ to $700 \mu s$. Left : particle behavior. Right : pressure distribution.

The left side of figures 1 to 4 shows the behavior of explosive particles while the right side shows the shock wave propagation. It can be confirmed that the propagation of the shock wave reaches the predetermined domain at $700 \mu s$.

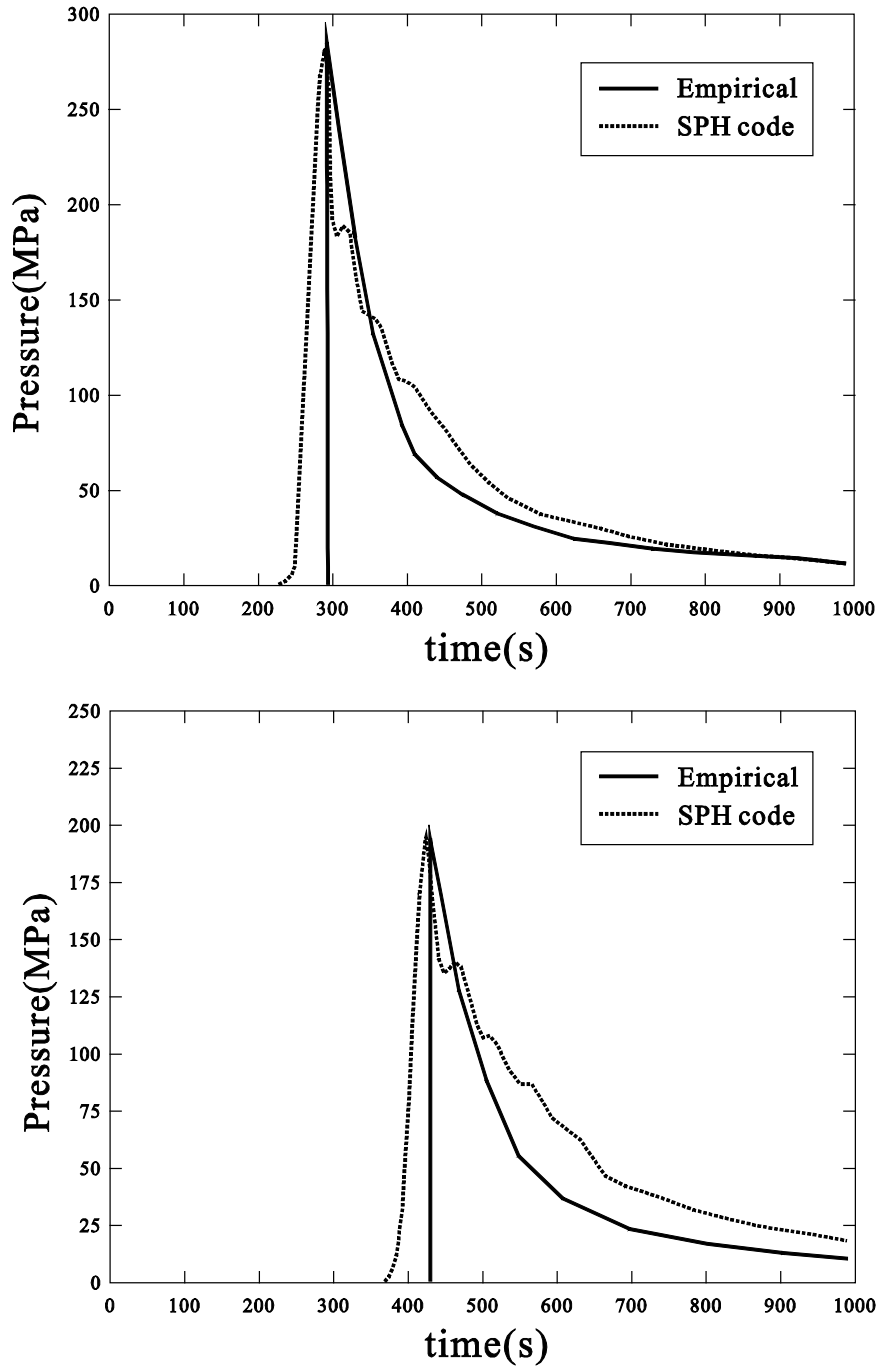


Figure 3.10. Comparison curve of shock wave pressure at gauging point 1 and point 2. Upper graph represents the gauging point 1 while lower graph shows the gauging point 2.

Fig.2 shows the compared results between numerical one and empirical one. The tendency of simulation curve shows good agreement with Zamyshlyayev empirical formulation[23]. The error may be caused by

accumulating the numerical error, and energy dissipation from using artificial viscosity. Nevertheless, the overall results show good behavior.

3.3 Bubble Rising Simulation

For the bubble rising simulation, there are restrictions on implementation using original SPH formulation. As mentioned in chapter 2, in the case of multi-phase problems with large differences in density, such as gases and liquids, it is difficult to maintain continuity in the calculation of the density variations using the continuity equations. Therefore, the simulation is performed using the formulation based on the volume approximation.

The Tait equation is used as the pressure state equation, and the number of particles used is 90000. The mirror particle is used for the boundary condition. The parameters used in the numerical model are in Table 3.1.

Table 3.1. Parameters for bubble rising simulation.

Particle initial distance	0.00075	m
Domain L ×H	0.15×0.25	m
Bubble radius	0.025	m
Bubble center position (x, y)	(0.075, 0.05)	m
Water density	1000	kg/m ³
Gas density	1	kg/m ³
Reynolds number	1000	-
Kinematic viscosity ratio	128	ν_G / ν_W

The purpose of the bubble rising simulation is to implement and verify the multi-phase problem as the previous step to simulate the bubble pulsation problem.

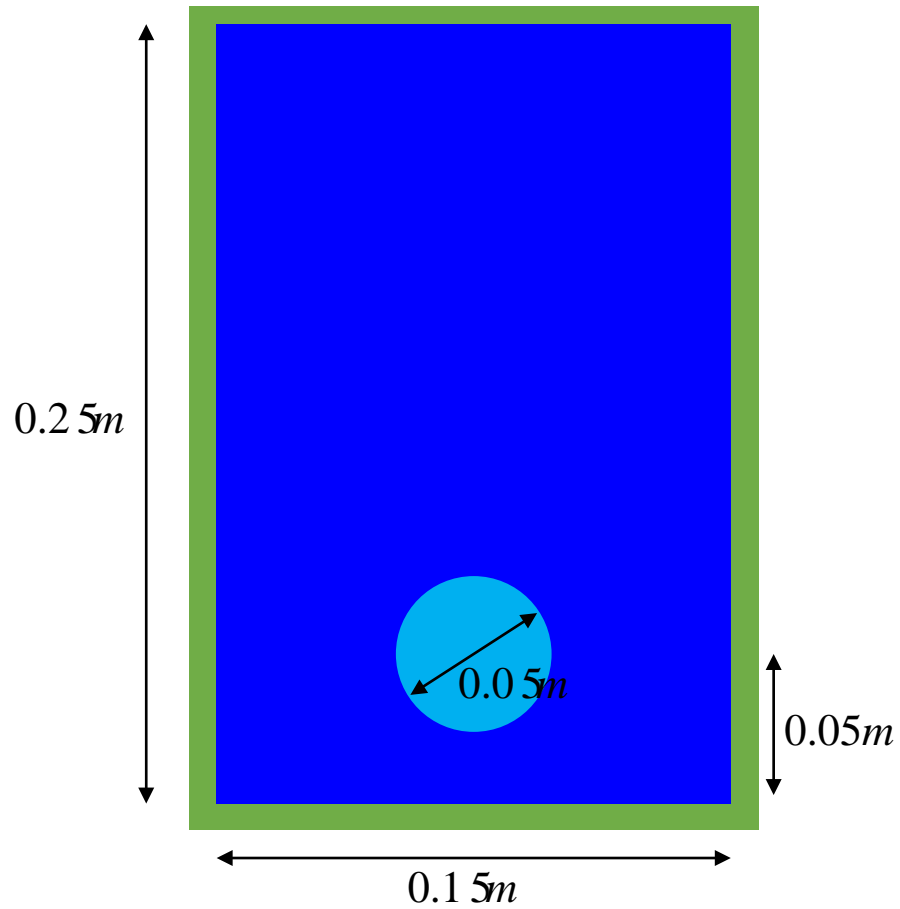


Figure 3.11. Numerical model of the bubble rising simulation. Green line represents wall boundary.

It is verified by comparing the results of other researchers using other SPH formulations and the Level-Set method. The Level-Set method[4,20] is based on FVM(Finite Volume Method) and is widely used in multi-phase research fields.

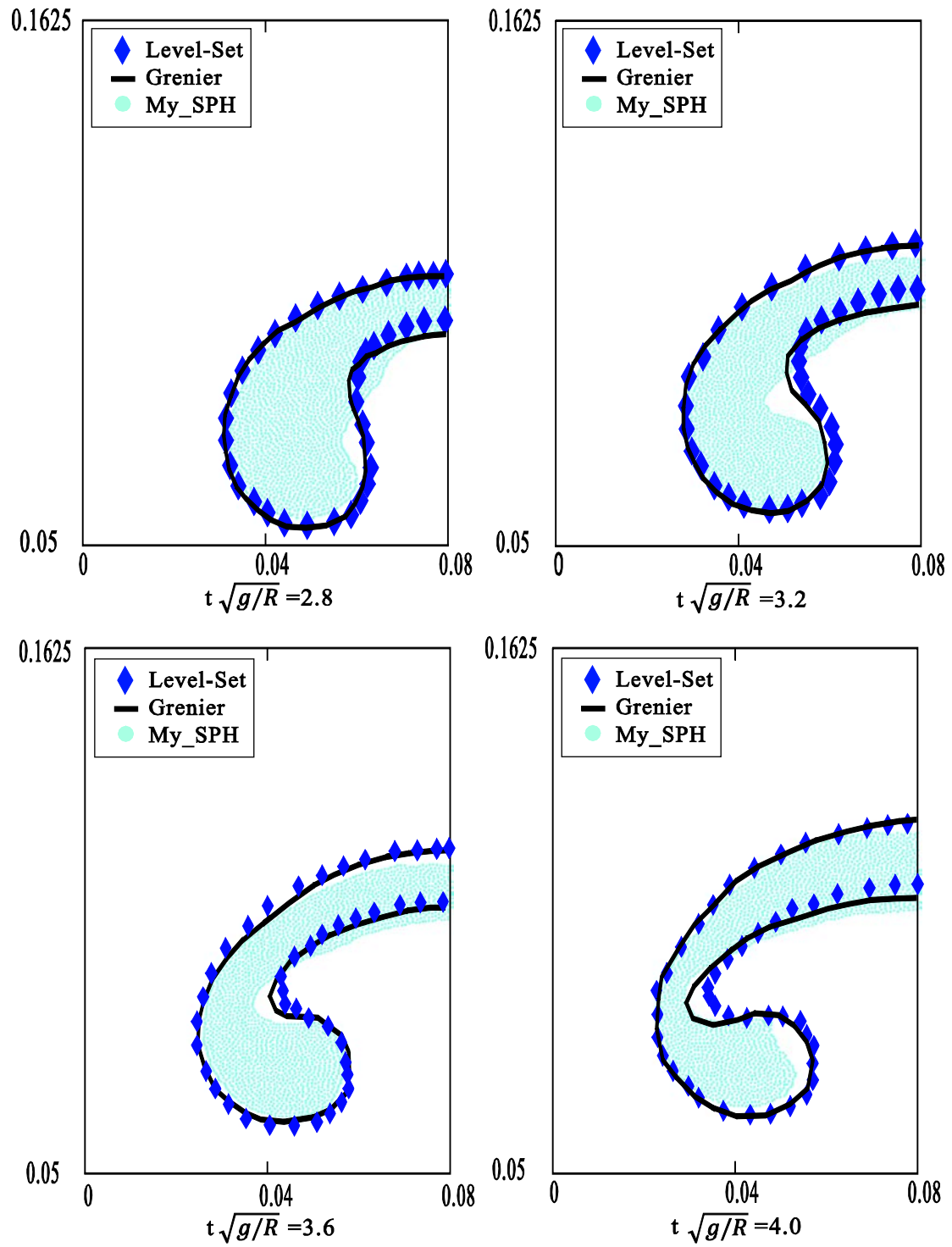


Figure 3.12. Comparison of bubble rising behavior from $t\sqrt{g/R} = 2.8$ to $t\sqrt{g/R} = 4.0$. Blue diamonds correspond to the Level-Set method[20] and black line represents SPH method proposed by Grenier[4]. Sky blue dots show the present SPH result.

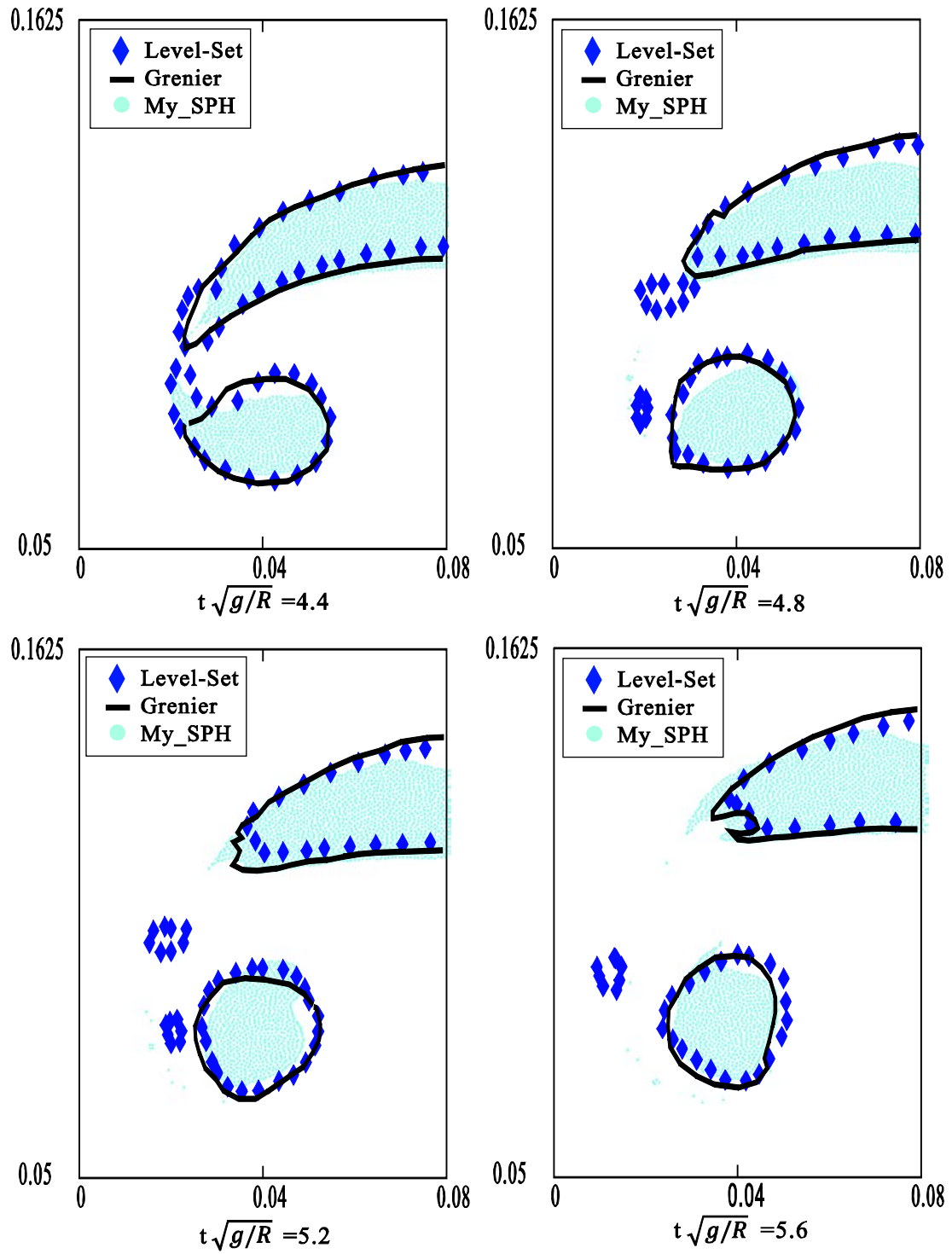


Figure 3.13. Comparison of bubble rising behavior from $t\sqrt{g/R} = 4.4$ to $t\sqrt{g/R} = 5.6$. Blue diamonds correspond to the Level-Set method[20] and black line represents SPH method proposed by Grenier[4]. Sky blue dots show the present SPH result.

The blue diamond corresponds to the Level-Set method, the black line represents other SPH formulation[4]. The sky blue circles show the result of this study.

In this study, the surface tension is not considered, so a slight difference may occur, but the overall behavior shows good agreement with other results.

3.4 Transition Point Verification

In this work, the transition point where the module is converted is proposed. The method uses an empirical formula. In other words, 3D shock wave simulation should be preceded to clarify the input value of the empirical formula.

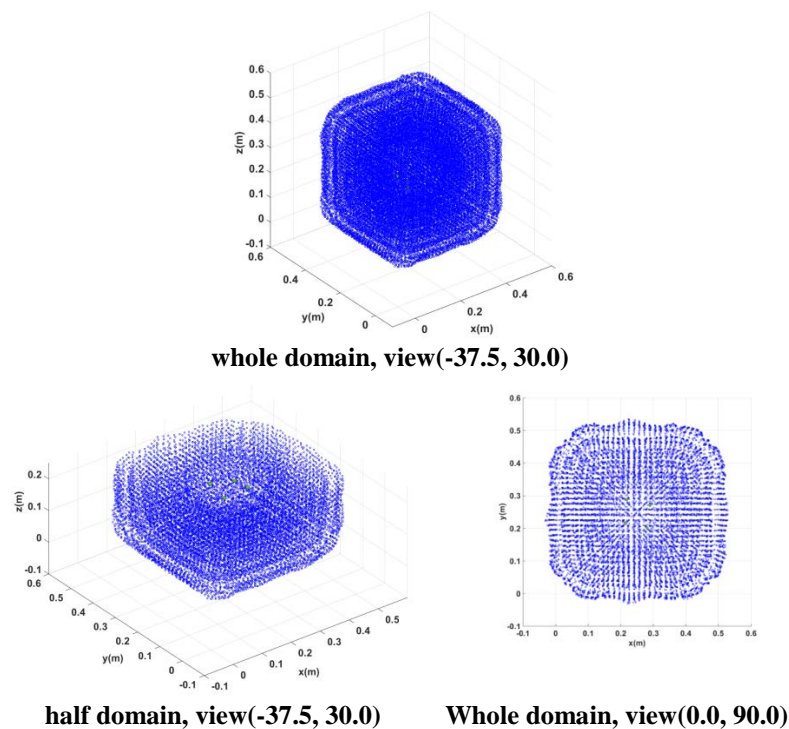


Figure 3.14. 3D shock wave simulation in three viewpoints. Clockwise from the top, view(-37.5, 30.0), half of view(-37.5, 30.0), view(0.0, 90.0).

Using $30 \times 30 \times 30$ particles, two cases for the 3D shock wave simulation are implemented. The input values of each case are as Table 3.2.

Table 3.2. Parameters for each case.

	CASE 1	CASE 2
Weight(W)	60.2(g)	483.0(g)
Domain (x×y×z)	0.5×0.5×0.5	1.0×1.0×1.0
Depth(D)	3.5(m)	3.5(m)
Explosive	TNT	TNT

To validate the transition point, the Rayleigh-Plesset equation in Equation (2.44) is used. The input values of the Rayleigh-Plesset equation, P_0 and R_0 , are obtained from the 3D numerical simulation of the shock wave. The reference pressure term of the Rayleigh-Plesset equation is calculated by the sum of atmospheric pressure(101.325 KPa) and hydrostatic pressure($\rho g D$). The results from the Rayleigh-Plesset equation are the maximal gas bubble size and the initial oscillation period. The result values are compared with those of empirical formula in Equation (2.2) that can be calculated by knowing the amount of explosives and the depth of explosion.

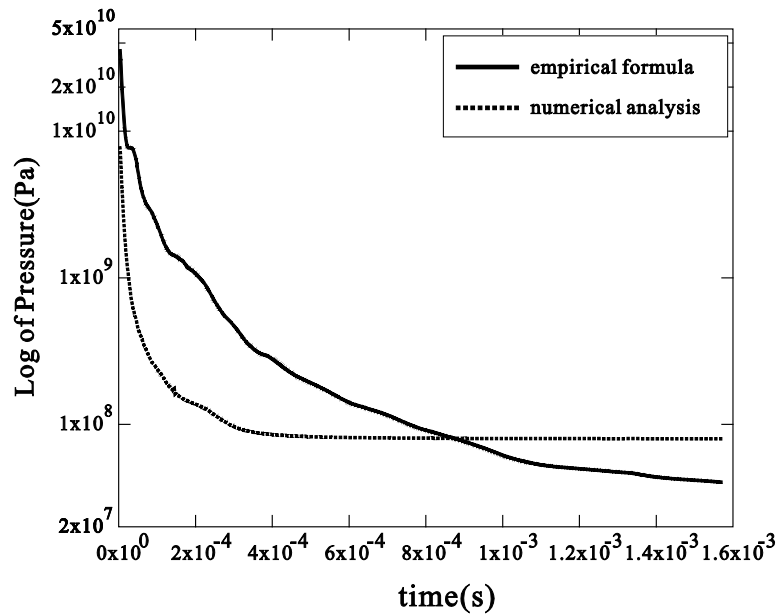


Figure 3.15. Log scale pressure comparison curve between empirical and numerical for CASE 1.

In the simulation of CASE 1, $P_0 = 80.330$ MPa and $R_0 = 4.46498$ cm is attained at 0.83ms. It can be seen in Figure 3.15.

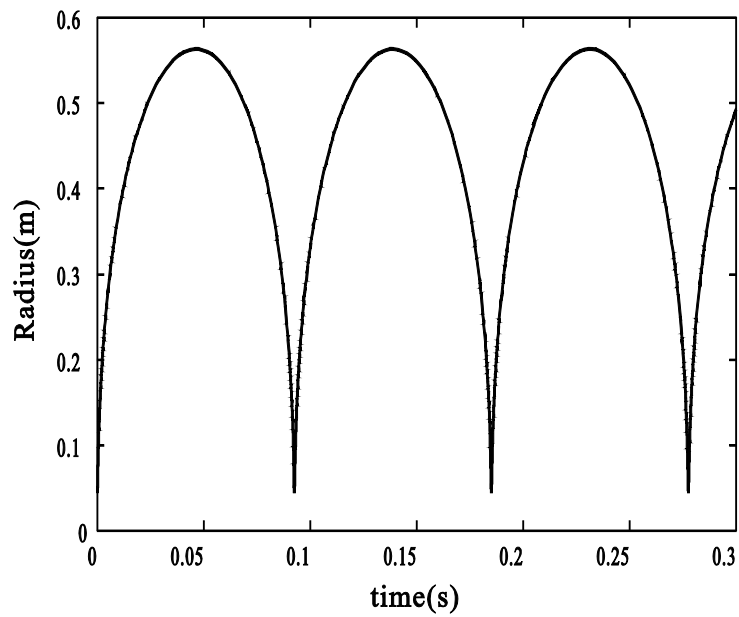


Figure 3.16. Rayleigh-Plesset curve for CASE 1.

The maximum gas bubble radius from the Rayleigh-Plesset equation is 0.5640m and the half initial oscillation period is 0.04565s. As a result of comparison with the empirical formula, the error is about 1 %.

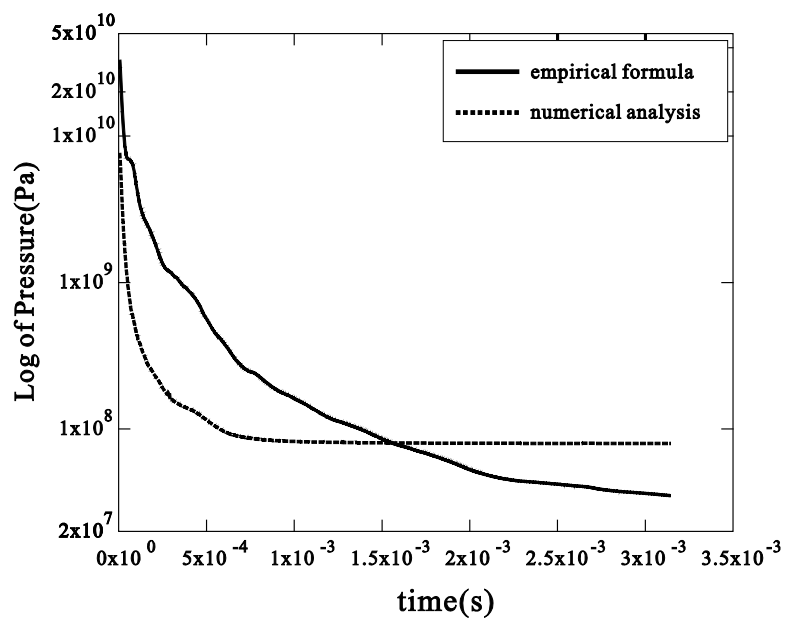


Figure 3.17. Log scale pressure comparison curve between empirical and numerical for CASE 2.

In the simulation of CASE 2, $P_0 = 80.477$ MPa and $R_0 = 8.92428$ cm is attained at 1.54ms. It can be seen in Figure 3.17.

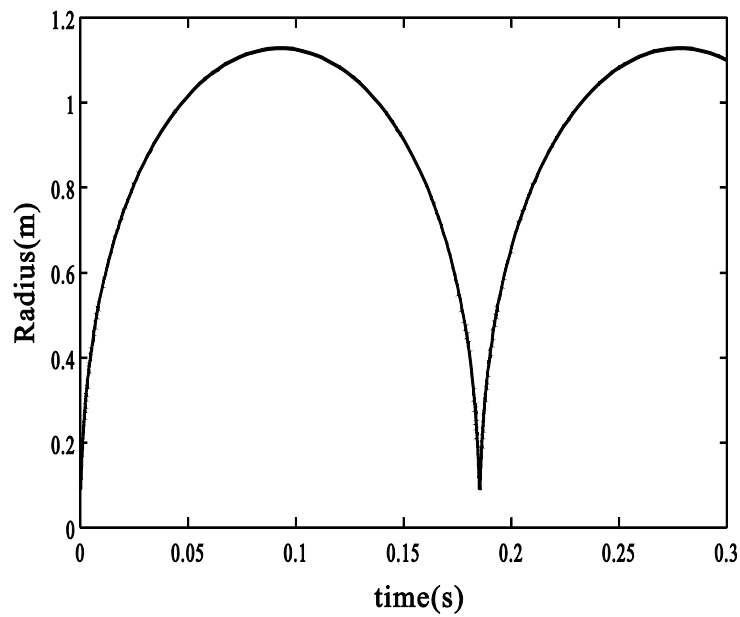


Figure 3.18. Rayleigh-Plesset curve for CASE 2.

For CASE 2, the maximum gas bubble radius from the Rayleigh-Plesset equation is 1.128m and the half initial oscillation period is 0.09118s. As a result of comparison with the empirical formula, the error is also about 1 %.

Table 3.3 represents the results comparing between the Rayleigh-Plesset equation and the empirical formula.

Table 3.3. Maximum radius and initial period comparison between the Rayleigh-Plesset equation and the empirical formula.

Time (ms)	$R_{max}(m)$		Relative error	$T_1/2(s)$		Relative error
	R-P equation	Empirical		R-P equation	Empirical	
CASE1	0.83	0.5640	0.0124	0.04565	0.04730	0.0349
CASE2	1.54	1.1280	0.0127	0.09118	0.09460	0.0362

As a result of the two case studies, it can be seen that the transition point proposed in this work shows the validity.

3.5 Bubble Pulsation Simulation

There are two ways to obtain the gas bubble radius at the initial maximum expansion state.

- (i) The way to get the maximum radius by substituting the pressure and radius obtained through the transition point into the Rayleigh-Plesset equation
- (ii) The way using an empirical formula in which the explosion depth and the amount of explosives are input values

Since the error of the maximum gas bubble radius attained from the two methods is about 1%, the average value of the two methods is used in this study. The simulation of the gas bubble pulsation phenomena using SPH has not been attempted so far, so various cases are tried for verification. First, the 2D case and the 3D case are compared. The numerical model parameter is as Table 3.4.

Table 3.4. Numerical model parameters for 2D CASE and 3D CASE.

	2D CASE	3D CASE	
The number of particles	90×210	60×140×60	
Domain	3.0×7.0 (L × H)	3.0×7.0× 3.0 (L × H ×B)	m
Bubble radius	0.561	0.561	m
Bubble center position	(1.5, 3.5) (x, y)	(1.5, 3.5, 1.5) (x, y, z)	m
Water density	1000	1000	kg/m ³
Gas density	1	1	kg/m ³
Reynolds number	1000	1000	-
Kinematic viscosity ratio	128	128	v_G/v_W

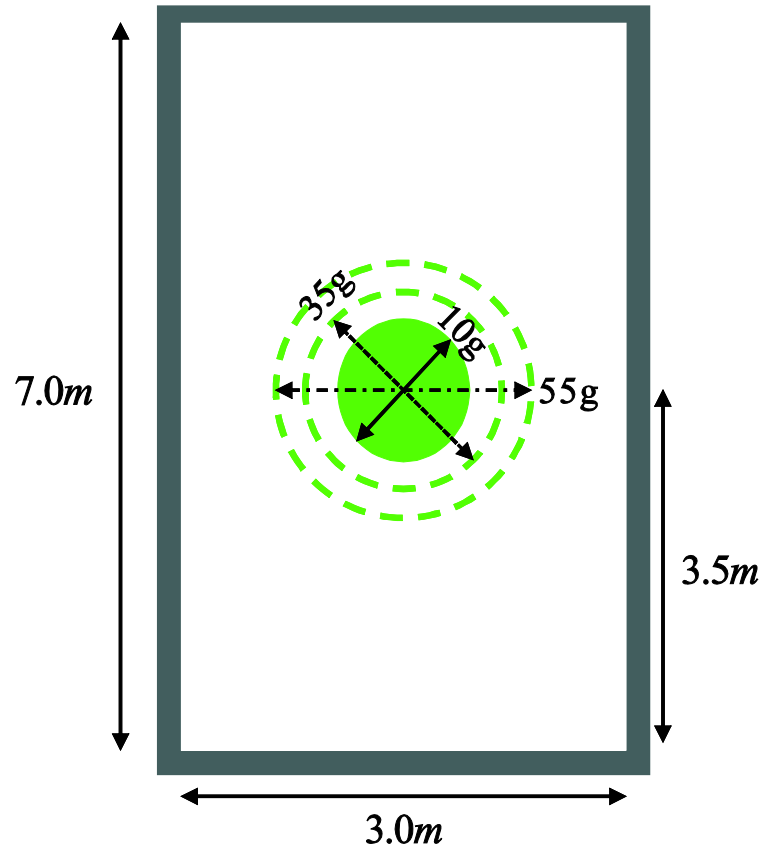


Figure 3.19. Numerical model of bubble pulsation

For 2D models, the volume calculation is not available. Therefore, the volume of a bubble sphere for 2D is assumed by the shape of a bubble circle. Thereby, the initial oscillation period of the gas bubble are compared. Prior to the implementation of the simulation, in the case of the 2D simulation, a cylindrical shape can be assumed if considering the thickness direction. It is therefore possible to predict that a longer period will occur compared to the 3D simulation.



Figure 3.20. Numerical results of a 55g explosive charge

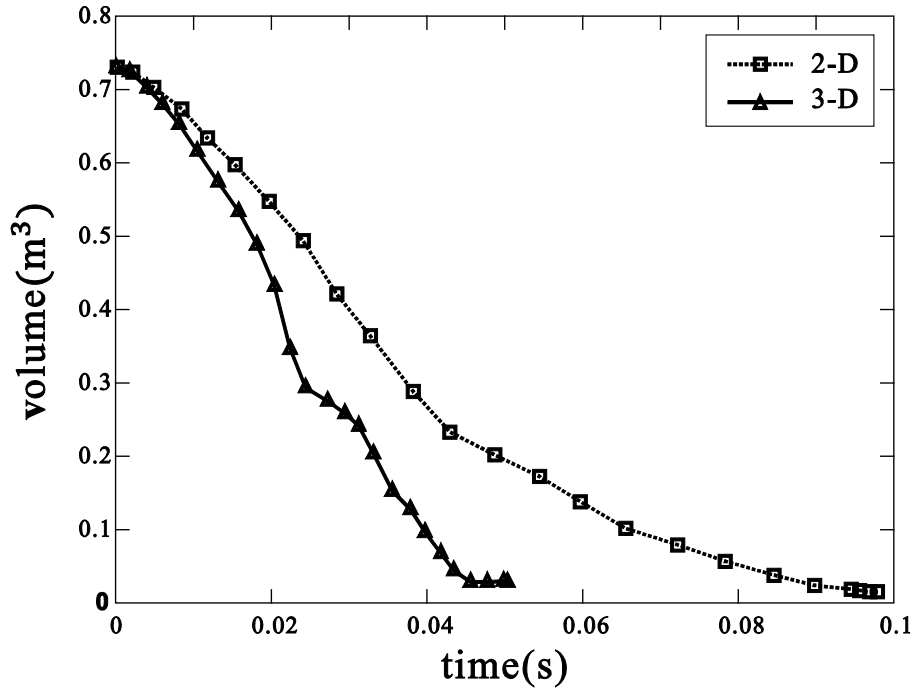


Figure 3.21. Numerical 2D(approximation) and 3D bubble volume profile for the explosive charge of 55g TNT.

Figure 3.19 shows that the 2D simulation shows a larger pulsation period than the 3D simulation, that is, the 2D simulation is different from the actual behavior. Therefore, 3-dimensional simulation is indispensable to implement the bubble pulsation behavior.

Next, the 3D model is simulated by increasing the number of particles. The parameters are the same as Table 3.4, and the number of particles used is $30 \times 70 \times 70$ (red line), $45 \times 105 \times 45$ (brown line), $60 \times 140 \times 60$ (green line), and $75 \times 175 \times 75$ (blue line). The simulation results are verified by comparing with the experimental results and the BEM(boundary element method)[9].

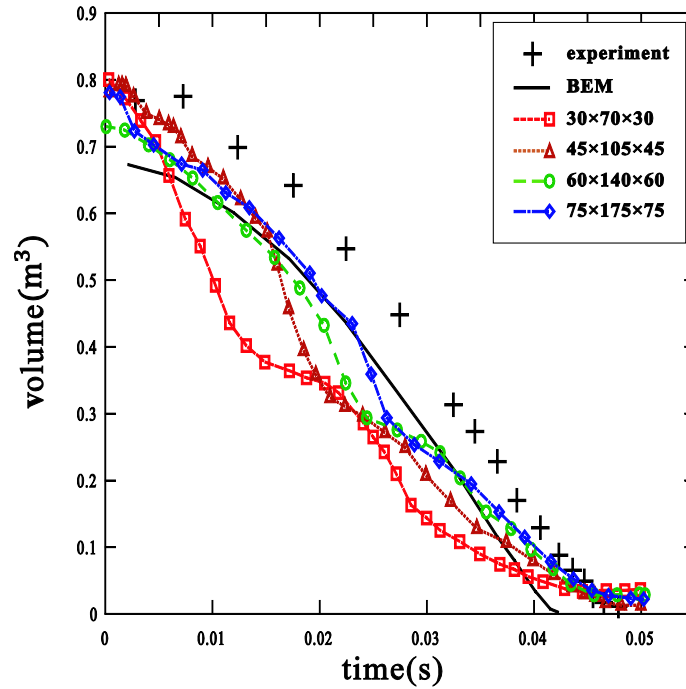


Figure 3.22. Time history of bubble volume with different number of particles. And comparison with experiments and BEM[9].

It can be shown that as the number of particles increases, it approaches the reference values (experimental results and BEM) more and more. This is the similar tendency as in the analysis using the conventional grid based methods. The grid based methods also show a better solution when using a finer grid

Lastly, the simulations for three cases where the amount of explosives used is different, that is, the maximum gas bubble radius is different are performed. The amount of explosive in each case is 10g, 35g, 55g respectively. $60 \times 140 \times 60$ particles are used for the simulation. Verification is carried out through comparing with experimental results and BEM results[9]. The cross mark corresponds to the experiment result and the black line represents the BEM results.

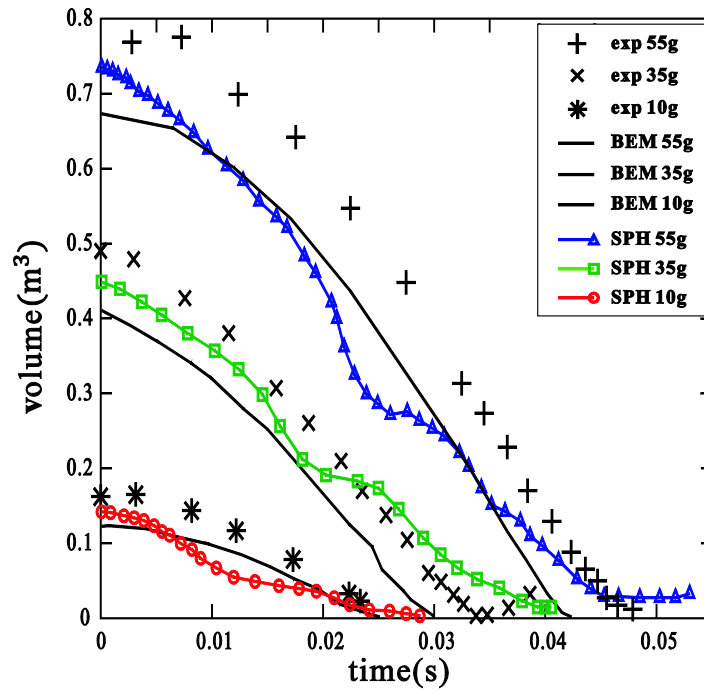


Figure 3.23. Time history of bubble volume with different amount of explosive charge. And comparison with experiments and BEM[9].

In the gas bubble pulsation simulation using SPH, it can be shown that the more the explosive amount is used, the longer the oscillation period is, such as the reference.

Chapter 4. Concluding Remark

In this study, several conclusions are drawn as follows.

- (i) Two main physical phenomena of underwater explosion are defined in terms of numerical analysis. Propagation of the shock wave is induced by instantaneous compression of the fluid. On the other hand, in case of gas bubble dynamics, fluid behaves close to incompressible flow. Also, for shock physics, the phenomenon is observed in microsecond-scale, while the gas bubble dynamics phenomenon behaves in millisecond-scale. Because of these differences, a numerical module suitable for each phenomenon is presented.
- (ii) Through a method proposed in this study, the point of transition from shock physics to gas bubble dynamics can be figured out. Since the numerical module is separated according to the physical phenomenon, a method for obtaining the transition point where the module is converted is required. In this work, an empirical equation is introduced for the numerical analysis to determine the transition point from shock physics to gas bubble dynamics. The validity of this method is verified by comparing with the Rayleigh-Plesset equation and the other empirical formulas.
- (iii) Modified Tait equation is proposed to implement the gas bubble pulsation phenomenon. The basic Tait equation represents the compressibility of the fluid, and the atmospheric pressure and hydrostatic pressure are added to calculate the pressure of the surrounding fluid. As a result of the calculation using the modified pressure term, the change of the radius of the gas bubble and its period are compared with the experimental results and the BEM-based numerical analysis results.

In the future work, the initial gas bubble expansion phenomenon which is not presented in this study due to the penetration phenomenon of gas particles should be implemented. And, the bubble jet that occurs after gas bubble pulsation should also be implemented.

Chapter 5. Bibliography

1. Colagrossi, A. and M. Landrini, *Numerical simulation of interfacial flows by smoothed particle hydrodynamics*. Journal of Computational Physics, 2003. **191**(2): p. 448-475.
2. Das, A.K. and P.K. Das, *Bubble evolution and necking at a submerged orifice for the complete range of orifice tilt*. AIChE Journal, 2013. **59**(2): p. 630-642.
3. Gingold, R.A. and J.J. Monaghan, *Smoothed particle hydrodynamics: theory and application to non-spherical stars*. Monthly notices of the royal astronomical society, 1977. **181**(3): p. 375-389.
4. Grenier, N., et al., *An Hamiltonian interface SPH formulation for multi-fluid and free surface flows*. Journal of Computational Physics, 2009. **228**(22): p. 8380-8393.
5. HA, D.M., *Numerical study of plunging wave in deep water*. 2010.
6. Hu, X. and N.A. Adams, *An incompressible multi-phase SPH method*. Journal of computational physics, 2007. **227**(1): p. 264-278.
7. Hu, X.Y. and N.A. Adams, *A multi-phase SPH method for macroscopic and mesoscopic flows*. Journal of Computational Physics, 2006. **213**(2): p. 844-861.
8. Hysing, S.-R., et al., *Quantitative benchmark computations of two-dimensional bubble dynamics*. International Journal for Numerical Methods in Fluids, 2009. **60**(11): p. 1259-1288.
9. Klaseboer, E., et al., *Experimental and numerical investigation of the dynamics of an underwater explosion bubble near a resilient/rigid structure*. Journal of Fluid Mechanics, 2005. **537**: p. 387-413.
10. Liu, G.-R. and M.B. Liu, *Smoothed particle hydrodynamics: a meshfree particle method*. 2003: World Scientific.
11. Liu, M. and G. Liu, *Smoothed particle hydrodynamics (SPH): an overview and recent developments*. Archives of computational methods in engineering, 2010. **17**(1): p. 25-76.
12. Liu, M., G. Liu, and K. Lam, *A one-dimensional meshfree particle formulation for simulating shock waves*. Shock Waves, 2003. **13**(3): p. 201-211.
13. Liu, M., et al., *Smoothed particle hydrodynamics for numerical simulation of underwater explosion*. Computational Mechanics, 2003. **30**(2): p. 106-118.
14. Meister, M. and W. Rauch. *Simulating rising bubble problems with smoothed particle hydrodynamics*. in *IMA Conference on Mathematical Modelling of Fluid Systems*. 2014.
15. Monaghan, J., *Smoothed particle hydrodynamics and its diverse applications*. Annual Review of Fluid Mechanics, 2012. **44**: p. 323-346.
16. Monaghan, J. and A. Kocharyan, *SPH simulation of multi-phase flow*. Computer Physics Communications, 1995. **87**(1): p. 225-235.
17. Monaghan, J.J., *Simulating free surface flows with SPH*. Journal of computational physics, 1994. **110**(2): p. 399-406.
18. Reid, W.D., *The Response of Surface Ships to Underwater Explosions*. 1996, DTIC Document.

19. Staroszczyk, R., *Simulation of dam-break flow by a corrected smoothed particle hydrodynamics method*. Archives of Hydro-Engineering and Environmental Mechanics, 2010. **57**(1): p. 61-79.
20. Sussman, M., P. Smereka, and S. Osher, *A level set approach for computing solutions to incompressible two-phase flow*. Journal of Computational physics, 1994. **114**(1): p. 146-159.
21. Szewc, K., J. Pozorski, and J.-P. Minier, *Simulations of single bubbles rising through viscous liquids using smoothed particle hydrodynamics*. International Journal of Multiphase Flow, 2013. **50**: p. 98-105.
22. Wang, L., et al., *Study on load characteristics of underwater explosion using RKDG-LS-DGF and BEM*. Shock and Vibration, 2015. **2015**.
23. Zamyshlyayev, B.V. and Y.S. Yakovlev, *Dynamic loads during underwater explosion*. Sudostroenie, Leningrad, 1967: p. 387.
24. Zhang, A., P. Sun, and F. Ming, *An SPH modeling of bubble rising and coalescing in three dimensions*. Computer Methods in Applied Mechanics and Engineering, 2015. **294**: p. 189-209.
25. Zhang, A., Y. Wen-shan, and Y. Xiong-liang, *Numerical simulation of underwater contact explosion*. Applied Ocean Research, 2012. **34**: p. 10-20.
26. Zhang, A.M., et al., *Numerical simulation of column charge underwater explosion based on SPH and BEM combination*. Computers & Fluids, 2013. **71**: p. 169-178.
27. Zhang, A.-m., et al., *Influences of initial and boundary conditions on underwater explosion bubble dynamics*. European Journal of Mechanics-B/Fluids, 2013. **42**: p. 69-91.

Chapter 6. Acknowledgments in Korean

감사합니다.

Chapter 7. Curriculum Vitae in Korean

박 형 준
(Park, Hyung Jun)

School of Mechanical and Aerospace Engineering,
Department of Mechanical Engineering
Korea Advanced Institute of Science and Technology
219 Daehak-ro, Yuseong-gu, Daejeon 305-701, Republic of Korea
(E-mail) hjpark89@kaist.ac.kr

Education

2005. 3. - 2008. 2. Pyeongchon High School, Anyang, Korea

2009. 2. - 2015. 2. INHA University, Incheon, Korea

B.S Department of Naval architecture & Ocean engineering.

Presentation

1. Park HJ, Kim HJ, Lee Ps, Chung H. The comparison of numerical simulation and experiment for fluid response of underwater explosion. Naval Ship Technology Seminar 2016.

Research Interest

Smoothed Particle Hydrodynamics, Underwater Explosion, Bubble dynamics

Skills

Computer programming skills : Fortran, MATLAB, C++